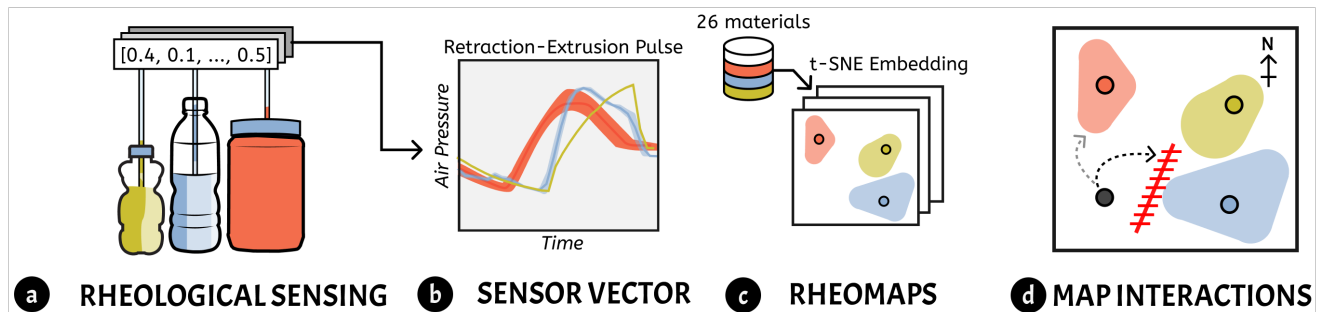




# RheoMap: Mapping Inks, Gels, Pastes, and Slurries within a Rheological Embedding Space using Retraction-Extrusion Pressure Sensor Vectors

Hoang Vuong  
The Hybrid Atelier  
University of Texas at Arlington  
Arlington, Texas, USA  
hxv6892@mavs.uta.edu

Cesar Torres  
The Hybrid Atelier  
UT Arlington  
Arlington, Texas, USA  
cearto@uta.edu



**Figure 1:** (A) Viscous materials such as honey, water, and peanut butter are pneumatically retracted and extruded through an air tube; (B) air pressure readings collected during this process are used to generate sensor vectors that encode distinct rheological information; (C) a repository of 26 viscous materials with 12 sensor vectors is used to construct a rheological embedding space, or RheoMap; (D) reference materials serve as landmarks to design interactive tools for navigating the rheological space.

## Abstract

Viscous materials such as inks, gels, pastes, and slurries are ubiquitous across domains like food science, smart materials, digital fabrication, and the arts. However, their dynamic and unpredictable behavior—shifting over time and in response to environmental factors—poses challenges, often requiring costly equipment for accurate rheological analysis. This paper presents a low-cost, accessible sensing routine that retracts and extrudes viscous materials through an air tube, generating sensor vectors rich in rheological data. By embedding data from 26 rheologically diverse materials into a two-dimensional space, we create RheoMaps that allow for tracking material changes over time, distinguishing concentrations, and tuning rheological behaviors. These maps offer practical benefits for detecting preparation errors, guiding material design and documentation, and providing tutorial waypoints. We further discuss how this approach can be extended to extract relational insights from sensor data, improving material literacy and manipulation across a range of applications.

## CCS Concepts

• **Computer systems organization** Sensors and actuators; • **Human-centered computing** Interactive systems and tools.

## Keywords

rheology, viscosity, material sensing, digital fabrication

## ACM Reference Format:

Hoang Vuong and Cesar Torres. 2025. RheoMap: Mapping Inks, Gels, Pastes, and Slurries within a Rheological Embedding Space using Retraction-Extrusion Pressure Sensor Vectors. In *CHI Conference on Human Factors in Computing Systems (CHI '25)*, April 26–May 01, 2025, Yokohama, Japan. ACM, New York, NY, USA, 24 pages. <https://doi.org/10.1145/3706598.3713835>

## 1 Introduction

In digital fabrication, the ability to manipulate and handle diverse materials such as liquids, inks, pastes, slurries, and gels is becoming increasingly important as the field expands beyond plastics. This evolution introduces more complex, functional, aesthetic, and sustainable material options, particularly through advancements in 3D printing technologies. Viscous mediums, unlike their plastic counterparts, are much more stubborn to work with. The materials are more prone to change from often unintended chemical and physical processes such as curing, drying, decaying, melting, or falling out of suspension. With these more dynamic characteristics, such materials require a different level of quality control, care, patience and understanding [4]. Expertise in handling such materials



is often the domain of *material whisperers* — those with both hands-on skills and theoretical knowledge to address the interdisciplinary demands of design, engineering, computation, material science, and manufacturing.

Several factors further complicate working with viscous materials beyond their dynamic behaviors. Ambiguities in protocols or unclear instructions can exacerbate these challenges, leading to issues with material compatibility, consistency, and dispersion [12, 38]. When working with rheological modifiers, such as thickeners or thinners, many practitioners are left to rely on subjective observations of before-and-after effects. Unfortunately, these insights are rarely documented, often forgotten over time, and difficult to replicate [37]. While sensor readings can provide immediate data on a material’s properties, they often require a wide breadth of costly equipment (e.g., viscometer, texture analyzer, rheometer) and fail to capture how different materials relate, interact, and perform under varying conditions. Scientific scales, such as the viscosity range of honey (2,000 to 10,000 cP), demand significant recall and expertise, adding yet another layer of complexity to the process.

As a result, integrating these materials into digital fabrication and more broadly within tangible computing, material-centered design, and human-food interaction pose substantial challenges. To better navigate this evolving landscape and support work with viscous mediums in HCI, new approaches are needed for troubleshooting and engaging with these materials such as inks [20, 34, 36, 56], gels (silicone [38], gelatin [35], hydrogel [19], mousse [66]), pastes (biomaterials [2, 49], chocolate [21, 22, 24]), and slurries (clay [3, 29] and concrete [60]). These challenges highlight the need for a more accessible, systematic method for understanding viscous materials. This work contributes:

- **Rheological Sensing Routine.** Inspired by the action of drawing a milkshake through a straw (Figure 1A), we introduce a simple, low-cost rheology sensing technique that uses an off-the-shelf pneumatic system (Programmable Air - PA) and a sensing system (ThingPlus with Micro Pressure Sensor) to record pressure data as small material samples (20-50 mL) are retracted and extruded through interchangeable air tube probes, with minimal material loss (0-5 mL). These retraction-extrusion pressure pulses (REPs) provide a quick snapshot of a material’s rheological properties within 1-2 seconds (Figure 1B). The sensing technique requires no resetting and can be automated for cyclic sampling, making it highly efficient for both open-air and integrated applications. Formal characterization of the REPs demonstrates sufficient variability across different materials and reliable signal quality for various tasks, including classifying materials by their rheological behaviors, monitoring material stability over time (e.g., during curing or setting), and distinguishing fluid compositions (e.g., concentrations).
- **Rheological Embedding Space** By treating REPs as sensor vectors, we applied t-SNE to embed 12 sensor vectors of 26 viscous materials into a two-dimensional space (Figure 1C). This embedding spans a wide range of rheological types commonly used in digital fabrication, physical computing, and human-food interaction, providing a unified framework for comparing and analyzing material properties.

To enhance interpretability and relational insights, we generated **RheoMaps** from this embedding, extending the concept of latent space cartography (LSC) [27] from its traditional application in semantic spaces to a physically grounded, sensor-based domain. These RheoMaps are used to demonstrate the practical utility of the embedding space, offering a clear visual tool for analyzing and interpreting rheological data.

- **Dynamic Mapping Interaction** Coupled with easy-to-obtain REP sensor vectors, RheoMaps can be used to uniquely serve as an actionable tool that can be integrated into making and fabrication workflows. Unlike traditional static visualizations, RheoMaps allow practitioners to plot new data points, situating their materials within rheological space in real time (Figure 1D). We demonstrate three dynamic mapping interactions: (1) *neighborhood mapping* enables verification of critical properties such as extrudability by determining whether a material aligns with the appropriate cluster of rheologically similar materials; (2) *route guidance and detours* allows practitioners to evaluate the effects of modifiers such as thickeners or thinners or processes like curing, observing shifts towards target reference material landmarks; and (3) *rheofencing* enables real-time monitoring of material behavior during processing, detecting if a material deviates from a target rheological region.

In this paper, we first review sensing and sensemaking techniques for working with viscous materials in HCI. Next, we introduce the REP sensing routine and our RheoMap generation method. We then present a set of RheoMaps and their characterization, and demonstrate how these maps can be used in dynamic mapping interactions. Finally, we discuss opportunities to expand RheoMaps, including adding environmental factors like humidity and temperature as map layers, developing shared RheoMaps for ecological validation of material recipes across different users, materials, tools, and techniques, and improving documentation by incorporating reference waypoints.

## 2 Related Work

Material detection, classification, and characterization have a unique history within the HCI community. We review works within the tangible computing, ubiquitous computing, and digital fabrication communities that specifically work with material sensing and explore studies outside of HCI, especially in rheology, as the study of flow behavior, that focus specifically on fluid materials sensing.

### 2.1 Materials Sensing in HCI

Within HCI, the ability to explore the intricate connection between humans and materials has been spurred by innovations in physical computing and material science [47]. These efforts have sought to understand how technology can support human-material dialogue to enable new functional and aesthetic expressions [14, 57]. A consistent challenge, however, has been the diverse materials that have entered the purview of HCI practices. Niholt et al. described the need for Smart Material Interfaces (SMIs) that allowed users to dynamically alter material properties in response to stimuli such as

electricity, magnetism, and temperature, yet sensing and monitoring material properties remain an open question. Feinberg et al. [13] argued that interactions should prioritize the ability of designers to see and understand the potential of materials, or *material vision*.

A suite of sensing techniques shows promise toward achieving this vision, yet liquids and liquid-like materials are often left out of human-material interaction design. Liquid material sensing techniques show positive signs towards supporting material practices. Chi et al. [8] introduced a real-time, cost-effective, and minimal waste texture scanning technique capable of detecting the fluid states of slurry-like materials. Other techniques have improved the robustness of liquid sensing through contactless sensing. Leveraging the transparency of materials, SensiCut [11] and SpecTrans [50] applied optical sensing for contact-less material identification. Radio techniques such as WiFi/LiDAR sensing [6], mSense [63], and FG-Liquid [25] were used to demonstrate that electromagnetic material properties can be recovered from the reflection of radio frequency signals and used to detect materials in ubiquitous computing settings. Vibration and acoustic material sensing such as Vi-liquid [17], Akte-Liquid [54], and sound simulation with VR/AR [61] also demonstrated strong accuracy; however, these techniques remain limited to sensing static material. Within micro-electromechanical systems (MEMS), microcantilevers [39] have proved capable of odor and material sensing [43]. Despite advances in material sensing and its applications within HCI have been underexplored. Since many of the sensing techniques involve minimizing contact between the material and electronics, the ability to sense flow behaviors in liquids has been limited. Our technique leverages pneumatics to maintain the integrity of electronics, provide flexibility in its usage across a variety of fluid sensing conditions, and obtain rheological data previously uncaptured by prior work.

## 2.2 Conventional Measurement of Fluid Viscosity

In rheology, the measurement of a fluid’s viscosity, its resistance to flow or deformation, is a critical aspect of materials science, fluid dynamics, and many other fields. The flow rates of highly viscous fluids, such as honey, are considerably slower than those of low-viscosity fluids, like water. Several traditional methods for viscosity testing exist, each with its specific set of advantages, limitations, and most suitable applications (showed as in Figure 2). Some of the most common methods include rotational, capillary, falling ball, back-extrusion, and oscillatory viscometer [53].

Rotational, cone-and-plate and falling ball viscometers, are good for measuring for steady-flow conditions but may lack accuracy in complex behaviors, such as time-dependent materials; while oscillatory viscometers provide insights into visco-elastic properties but are limited in low-viscosity fluids and complication usage. The retraction-extrusion pulses generated using our system are similar to back-extrusion viscometry or capillary viscometer [10]; in contrast, our method draws materials into an air tube probe and subjects them to forces from changes in air pressure. The pressure is distributed over the cross-section of the air tube and material, thereby applying a shear force to the material upon extrusion. We

used a commercially accessible pneumatic system [51], which effectively minimizes material consumption, accomplishes prompt outcomes within a time frame of 1-2 seconds, and enables iterative testing to evaluate the system’s performance across multiple cycles.

Recent improvements in machine learning (ML) have opened up new ways to study rheology, especially in predicting how materials will behave. Mahmoudabadbozchelou et al. [31, 33] demonstrated that machine learning models could be used to identify complex rheological properties from a small dataset of cone-and-plate viscometer measurements. When coupled with a rheology-informed neural network (RhINN) [32], a few empirical measurements have been shown to be capable of recovering more constitutive models that explain how materials behave more generally to stress and strain. When formulating new materials, the Random Forest algorithm has shown value in identifying qualitative and physical factors in material formulas influencing the printability of hydrogels as soft ink and bio-ink materials [42]. While a promising route for material sensing, these models remain specialized. In-the-wild data collection is needed to adapt these models to a wider breadth of materials. We view our sensing technique working in synergy with machine learning approaches, specifically providing a feature rich rheological profile from a sensing mechanism that is repeatable, reproducible, precise, low-cost, and portable.

## 2.3 Latent Space Mapping

Latent space cartography has proven useful in helping users explore and verify relationships between data points in various domains. For instance, Liu et al. [27] demonstrated how users could discover connections within an emoji latent space by interacting with features like nearest neighbors or reprojecting the space along an attribute of interest. Similarly, VideoMap[26] applied latent space cartography to organize videos based on properties such as color, content, or motion, introducing interactions like districts, paths, and landmarks to support video editing. RecipeScape [7] expanded this concept into the culinary domain, creating a map for high-level exploration of recipes that visualized usage patterns through stacked trees and provided statistical displays of co-occurrence patterns.

While these methods have significantly improved the visibility and explainability of latent spaces, they primarily focus on exploring pre-existing data. What remains underexplored is how users can actively engage with latent spaces to generate new data points and use these spaces for sensemaking. This gap highlights the need for approaches that allow users not only to navigate and interpret latent spaces but also to actively contribute to and manipulate them for more meaningful insights.

## 2.4 Sensor Data Display

Traditionally, sensor data has been displayed using familiar methods such as classic readings and time series data (e.g., line graphs). While effective, these approaches often limit the ways in which users can interact with or interpret the data. Researchers have explored alternative ways of making sense of sensor data through data visceralization approaches. For instance, sonification has been used to provide auditory feedback during processes like crocheting, where the sound reflects the movement of the needle, encouraging

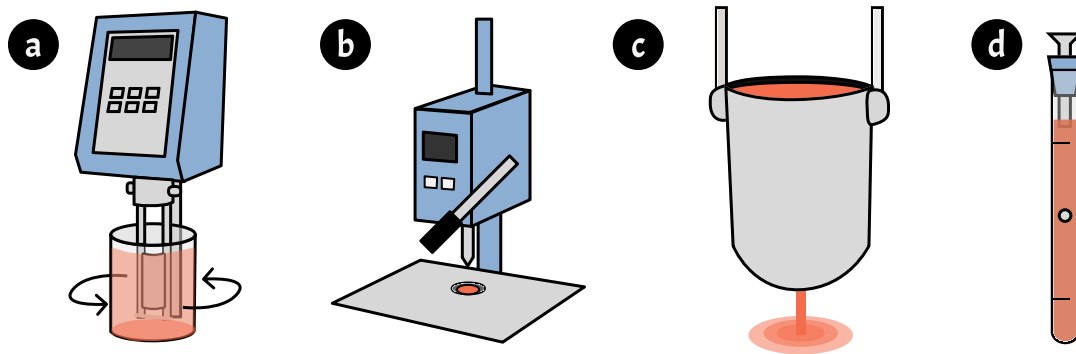


**Figure 2: Traditional Methods for Measuring Viscosity** Common industrial methods for viscosity measurement include: (A) A rotational viscometer, which determines viscosity by measuring the torque required to maintain a spindle’s constant speed in a liquid; (B) A cone-and-plate viscometer, which calculates viscosity based on the force needed to rotate a cone at a set speed while a small volume of liquid is positioned between the cone and a flat plate; (C) Capillary viscometry (flow cup), which measures the time it takes for a liquid to flow through a small hole at the bottom of a cup; (D) Falling ball viscometry, which determines viscosity by timing how long it takes for a ball to fall through a fluid under gravity [41].

practitioners to reflect on their craft [52]. Tian et al. [55] employed simulated ambient particles to visualize data, offering a more immersive and experiential way to engage with information, moving beyond the limitations of traditional graphs and bar charts. Sensor data from multiple sensors have been used to create spaces to facilitate greater sensemaking. For example, microfluidic chips have been utilized to juxtapose colorimetric responses for plant health diagnostics, visualizing critical metrics such as nitrate levels, pH, and hardness [28]. These novel approaches highlight a shift toward more embodied, interactive data representations. However, a gap remains in actively using sensor data to guide material processes in real time. While visualizations have advanced, direct integration of sensor feedback into workflows — beyond static readings and time-series graphs — presents a critical opportunity to explore how sensor data can shape and enhance material workflows dynamically.

### 3 Rheological Sensing Technique

Working with fluid, viscoelastic, or slurry materials presents distinct challenges due to their dynamic nature. These materials are especially temperamental — they can dry out, cure, become contaminated, or undergo rapid changes, making real-time monitoring essential. However, existing systems often lack the capability to capture the rheology of such materials at the moment of interest. To address these limitations, we designed RheoMap, a novel wireless sensing system to track rheological material inquiries using off-the-shelf components; to explore fluids interaction, enhancing our understanding and interaction with their properties for creative applications and fabrication in HCI.

#### 3.1 Sensing Rationale

Sensing rheological properties of materials requires a need to understand how material behaves under external forces. The challenge lies in how to apply a force to a uniform area of a *liquid or liquid like*

material sample (stress) and measure its deformation or displacement [30]. Our sensing technique is inspired by the back-extrusion technique where a material sample is deposited in a cylindrical receptacle that is unobstructed at its upper end [9, 16, 45]. A piston with a reduced diameter is then used to apply a force to the material, leading to its displacement into the space between the piston and the cylinder (annulus) [1]. Our approach uses a plastic air tube as a receptacle and pneumatic actuator as an "invisible" piston that can apply a constant force to both draw and expel material from the tube. The air tube ensures that forces are constrained to the cross-sectional area of the air tube, while pneumatic sensing allows us to indirectly measure material displacement by sensing the air pressure over time within the tube. For instance, the amount of time it takes for a material to be expelled (air pressure equal to atmospheric pressure) from the tube indicates how far the material traveled within the tube.

#### 3.2 Sensing Routine

The RheoMap sensing routine is driven by an off-the-shelf Arduino-based pneumatic system (Programmable Air (PA) [51]) that houses motor pumps for blowing, sucking, and venting operations. A separate air pressure sensor module (Qwiic MicroPressure Sensor) has a pressure detection range of absolute pressure from 0 to 30psi (206.84kPa). A WiFi-enabled microcontroller (ESP32 Thing Plus) is connected via serial to the Programmable Air’s Arduino Nano to support wireless sensing and data streaming. The sensing routine retracts and extrudes materials connected to the pneumatic system with a 100 cm tube with an inner diameter of 4.7 mm split evenly with a quick-release connector. We use a serial interface to specify material sample names; collected data from the sensing routine is then timestamped and saved to a csv file.

Air pressure readings are sampled at a rate of 20 samples per second (20 Hz); sampling occurs during a non-blocking delay (NBD).

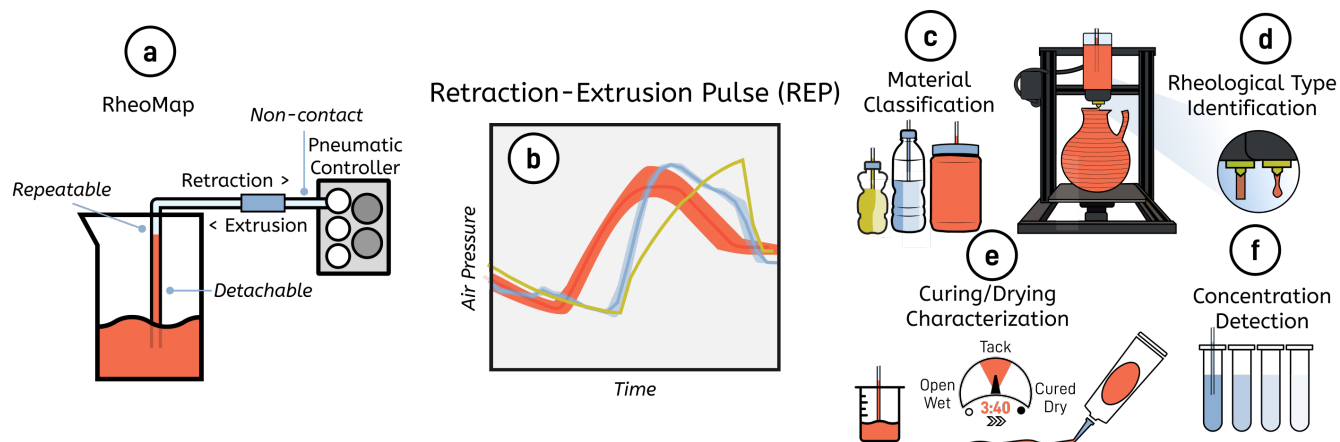


**Figure 3: Rheological Sensing.** (A) pneumatic retraction and extrusion for sampling fluid materials with detachable air tube probes; (B) by sensing air pressure over time, the method is capable of extracting a retraction-extrusion pulse (REP) that captures rheological properties of liquid materials; these REPs can be used to (C) support interactive material classification to support design practices, (D) detect rheological properties to support digital fabrication, (E) detect different material stages to support material practices, and (F) characterize concentrations of solutions for biomaterial fabrication.

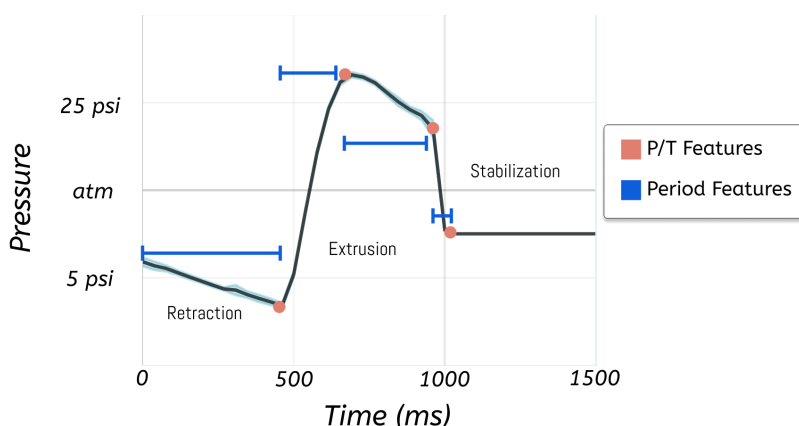


**Figure 4: The Retraction-Extrusion Pulse (REP) - Pressure and time (P/T) features are used to characterize how materials behave when retracted into an airtube probe and extruded at a constant rate. The sampling technique takes about 1000 ms; a short pause between samples is needed for the system to stabilize.**

- Probe Preparation** Insert an air tube probe into the quick connector (standard 4.7 mm ID, 100 cm). Submerge the probe into the material sample without touching the bottom of the container.
- Retraction** Set the vacuum motor to 100% power (2L/min) and sample during a 250 ms NBD.
- Extrusion** Set the pump motor to 100% power (2L/min) and sample during a 250 ms NBD.
- Cycling** To improve the reliability of the data, the routine can be repeated without intervention and support cycle testing. The same probe can be left in the material, rinsed and reused, or otherwise disposed for food-safe applications.

The 250 ms sampling interval was empirically selected as sufficient for capturing both high-viscosity (e.g., honey) and low-viscosity (e.g., water) samples within the probe segment of the

system. For portability and compatibility, a standard tubing size was used. The motor power was set to maximum (2L/min) to produce the strongest forces, allowing us to observe and analyze rheological behaviors effectively across materials.

*Calibration Routine.* To support diverse system configurations and sensing routines, we incorporated a calibration routine using water as a reference material to improve measurement accuracy. This routine involves comparing air pressure data from water samples in a new system setup (e.g., using different air tubes, motor power, or sensors) to data from our reference system. First, we extracted features computed based on statistical, shape, and frequency-domain by using mean, standard deviation, median, and dominant frequency. With those features, an error function were constructed

to apply a phase shift, scaling transformation, and intercept adjustments, minimizing the area difference between new and reference signals. To further enhance alignment, we used Polynomial transformation [5, 44] with 3 degree for amplitude scaling, capturing both linear and non-linear variations in the signal. K-means clustering ( $n=2$ ) from Scikit-learn [5, 44] was applied to group materials by intercept values and baseline offsets, enabling targeted intercept corrections based on the distinct characteristics of each fluid materials. We employed Powell optimization [44, 46] to minimize this error term, allowing us to learn an optimal scaling, phase shift parameters, intercept, and polynomial coefficients to better align the data. We then extracted features from new data and applied classification based on those feature with Random Forest [44] to predict the appropriate intercept adjustments, thereby aligning data more closely with the reference materials and tested the performance of our transformer and calibration. We applied train on the old configuration dataset; then test the new sensor data before and after transformed with split cross-validation across of calibration dataset with materials ( $n=5$ ). The evaluation showed an F1-weighted score 36% without calibration and 86.4% with calibration, which indicated the model's ability to maintain precision and recall across materials after calibration. Note that, the calibration routine is only necessary when the system has been reconfigured.

*Rationale.* Our sensing routine mirrors the rapid alternation between the suction and expulsion phases method proposed by Perrot et al. [45]. This pattern induces a continual flow and counter-flow within the material sample, generating rich data on the material's flow behavior and other rheological properties under variable stress conditions. In contrast to a mechanical piston, pneumatic actuation allows us to repeat measurements, reducing the need for extensive cleaning or re-calibration procedures, and further enhances the versatility and efficiency of rheological sensing.

*Limitations.* The system does not have a check valve to prohibit material backflow since the valve was observed to affect the air pressure readings. A short NBD and longer air tube probe are important to prevent motor damage. The power of the motors needs to also be commensurate with the size of the air tube; otherwise, it is possible for the material to escape the air tube probe. The Programmable Air motors are not food safe, therefore, it is recommended that food samples be disposed.

### 3.3 Data Cleaning and Feature Extraction

In order to extract REPs from sensor time series data, we first segmented the data into individual pulses. The pulse was marked when a running average was observed to deviate (start) and return to the baseline condition (end), respectively. For our experiments, the baseline range of 490 to 510 represented the system at equilibrium (atmospheric pressure; 10-bit resolution). A set of data validation checks were used to ensure the pulses were in acceptable ranges (e.g., duration, amplitude); lastly, collected pulses were padded and truncated appropriately to match the average pulse length; the pause in our sensing routine was used to ensure that only baseline values were padded.

We then extracted total 12 pulse features that could be used to represent the stress and strain of sampled material. As depicted in

Figure 4, the REP first captures the *retraction phase* – during this phase, the pneumatic vacuum is expelling air from the tube until enough of a pressure differential (retraction min) is achieved to cause the material to enter the tube (stress). Pressure will rise as the material is drawn further into the tube (strain). When entering the *extrusion phase* (stress), the REP shows two drops. The shorter drop describes the period in which the material is being expelled from the tube (strain), while the following more acute drop represents a *stabilization phase* where the system returns to equilibrium. The final feature set baseline, extrusion, retraction, and equilibrium phase sensor value ranges and time periods.

## 4 Sensor Routine Evaluation

Data collected from our sensing routine was stored in a sensor vector. We conducted a series of characterizations to understand the effectiveness of our sensing routine. First, we explored our sensing routine's *signal quality*. We examined the precision of the signal during cycle testing, identified the frequency of outliers for different material samples, and assessed the robustness of the system given different configurations. To understand the *material detection power*, we trained simple decision tree models to detect different rheological types and predict material properties such as viscosity, solution concentration, and curing stage. Lastly, we look at the overall *usability* of the technique and report the system's size and weight, cost, data management practices, collection times, and the interpretability of the results.

*Protocol.* The experiments described below follow a common experimental protocol for collecting retraction-extrusion pulses (REPs) from material samples using the RheoMap system:

- **Setup** Any residual material was first dispelled from the air tube probe by using the air pump to release the material into a waste beaker; the exterior of the air tube was wiped clean. Air tube probes (100 cm, 4.7 mm ID) were reused to emulate conditions. For stickier materials like peanut butter, the probe was repeatedly rinsed with soapy water.
- **Material Sample:** About 100 mL of a material sample (enough to submerge the air tube probe) was collected in a glass beaker. The air tube probe was suspended over the beaker using a beaker clamp; the probe was placed in the center of the material sampled, avoiding contact with the bottom of the beaker.
- **Data Collection:** Sensor readings were collected with a 1000 ms pause in between cycles to allow the material to settle; each sensing cycle lasted 1000 ms. Each sensing routine, unless otherwise noted, was sampled within 60 cycles. Collected data was annotated with a material description including the concentration of constituent parts (%), volume (mL) of the sample, length (cm) of the tube, pump power (%), type of container, liquid temperature, and qualitative notes. Collected data was streamed to a NoSQL database (MongoDB).

All resulting data was analyzed using computational notebooks (Google Collaboratory) that pulled sensor readings from the database into pandas data frames.

*Rheological Materials Dataset.* Inks, gels, pastes, and slurries are ubiquitous across domains in HCI and are often dynamic, tricky, and unpredictable. Understanding their behaviors and characteristics are essential when working with fluid materials in makerspaces. To ensure we covered a wide range of fluids and captured their representative properties, we used our sensing system to collect retraction-extrusion pulses (REPs) from different materials and analyze their rheological behavior.

A **classification dataset** was collected to evaluate the sensitivity of the sensing routine, comprising 26 unique material classes selected for their distinct rheological behaviors, including liquids with three levels of viscosity (inks, syrups, thick), mediums with non-newtonian properties (gels, pastes), and compositions with large and fine particles in suspension (slurries) (see Figure 5). A total of 1.2k pressure readings (REPs) were recorded.

## 4.1 Signal Quality

*Measures.* To measure the *precision* of the retraction-extrusion pulses and ascertain the noise level in the signal, we used Peak Signal-to-Noise Ratio (PSNR) to measure the noisiness of the REP pulses. Given a set of REP pulses for a given material  $m$ , we treated the mean REP pulses as the representative signal  $\hat{m}$ , and quantified noise using the Mean Squared Error (MSE) as follows:

$$\text{MSE}(m) = \frac{1}{t} \sum_{i=1}^t (m_i - \hat{m}_i)^2 \quad (1)$$

The PSNR value for each class was computed as:

$$\text{PSNR}(m) = 20 \cdot \log_{10} \left( \frac{\max(m)}{\sqrt{\text{MSE}(m)}} \right) \quad (2)$$

where  $\max(m)$  is the maximum intensity value of the signal. As a rule of thumb, a PSNR value of 20dB or lower is considered poor, while a 40dB or higher value is deemed excellent.

To further understand the *reliability* of the sensor during sampling, we conducted a cycle test to detect outliers. Each material was sampled consecutively for 60 trials. We examined the min retraction and max extrusion pressure within a material class and detected outliers using the 1.5 \* interquartile range (IQR) method.

PSNR and outlier rates were computed for our material space dataset  $M$  ( $|M| = 26$ ;  $n=60+$  samples each), different configurations of our system, and samples there taken 30 days apart.

*Material Range.* Across 26 different materials, the average PSNR value was found to be  $40.4 \pm 6.6$  dB with an outlier rate of 6.9%. Specifically, the PSNR reached as high as 43 dB for Newtonian materials; this trend is corroborated by the small outlier rate found in canola oil and water samples; tomato sauce and honey also exhibited smaller outlier rates (2%). In contrast, the PSNR values of dilatant and thixotropic materials like lotion and jam were notably lower, ranging between 31 and 32 dB. More viscous materials like peanut butter and hot fudge exhibited an outlier rate of 14%; this could be attributed to both limitations in the power capabilities of the system, but also to the proclivity of these materials to trap air bubbles; notably, thixotropic materials and dilatant materials exhibit increased or decreased viscosity, respectively, with different shear rates; since forces as applied when extruded, these behaviors can be used to explain the greater variability. These behaviors are further

reinforced by Figure 7 which depicts how the majority of the noise occurred during the extrusion phase of the REP pulses. In retrospect, features derived over repeated REP pulses with different forces, such as PSNR, could be useful to improve the ability to discriminate between thixotropic and dilatant materials. For further analysis, we applied the classic material classification method, Random Forest [44], based on features extracted from REPs across all materials. The model successfully classified different materials based on their feature characteristics, achieving an accuracy score of up to 96% cross validation (see in Figure 6).

*Durability.* First, to gauge the durability of the system in maintaining signal quality, we performed periodic material sampling, with 30-day intervals between sessions. A PSNR value of 12 dB was observed. The REP (Figure 7) indicate that raw sensor data is subject to periodic drift; the distance when projected on PCA space still indicate that water, milk, and honey had a 88%, 79%, and 57% similarity with its earlier counterpart, respectively.

When comparing the REP of water sampled with a lower motor power (Figure 7) versus the original and 30-day REPs, it appears that part of the noise can be attributed to degradation in the Programmable Air itself. This indicates that for REPs to be reliable, it is best to capture the REPs of reference solution in the same sensing session. The calibration process was simplified using a pressure sensor (SparkFun Qwiic MicroPressure Sensor), which is self-calibrating. Specifics regarding calibration can be found in the datasheet and user's manual for the PA and pressure sensor [15].

We observed that while the system consistently produced similar REP signals, it experienced periodic drift over time, with a PSNR of 12 dB for samples collected over 30 days. Specifically, motor power degradation was observed, which could affect the system's long-term stability.

*System Configurations.* Two different system configurations were tested. The first involved using a larger air tube probe (8 mm - 3/8" ID); this would alter the shear rates that could be applied on a given sample – consequently, this caused a low PSNR of 19 dB and an outlier rate of 30.6%. This significant reduction highlights the need to adjust the system to achieve target shear rates. With the Programmable Air, the air tube probe needs to be smaller than (4 mm - 3/16" ID) with the max pump and vacuum power. The second used an inline check valve that plays a crucial role in controlling fluid flow and averting reverse flow that can damage electronic system. The poor signal quality (19 dB) indicate that standard "duckbill" check valves are incompatible with the technique since they impede airflow and therefore pressure readings.

*Calibration.* To address system robustness and durability issues, we applied a calibration routine similar to the one described in Section 3.2 to evaluate system performance under different configurations. This evaluation was conducted on five fluid materials—milk, canola oil, honey, ketchup, and hot fudge—alongside water as a reference material. These materials were selected to capture a broad range of viscosity and flow behaviors, ensuring generalization across diverse material properties. The system was tested under two distinct sensing configurations: (1) a (2.4 mm - 3/32" ID) small tube and (2) a reduced power configuration with

REPs ID	Material	Rheological Type	Function Type	Viscosity (cps)	Preparation Notes
	Water	Newtonian	<b>Ink</b>	1	Tap Water
	Milk	Newtonian	<b>Ink</b>	3	Whole Milk
	Canola Oil	Newtonian	<b>Syrup</b>	100	Kroger
	Gelatin	Newtonian	<b>Gel</b>	500	Jell-o brand; 2:1 boiling water to gelatin; stir for 2 minutes. Add 2 parts cold water and stir for 2 minutes; refrigerate.
	Ketchup	Pseudoplastic	<b>Pastes</b>	10000	Great Value
	Egg White	Pseudoplastic	<b>Syrup</b>	2250	Separated from whole egg
	Shampoo	Pseudoplastic	<b>Pastes</b>	2500	Old Spice
	Tomato Sauce	Pseudoplastic	<b>Pastes</b>	2600	Prego
	Honey	Pseudoplastic	<b>Thick</b>	3000	Local Texas Honey
	Corn Syrup	Pseudoplastic	<b>Syrup</b>	3500	Karo
	Greek Yogurt	Thixotropic	<b>Gels</b>	5000	Oikos Pro 0% fat
	Hand Lotion	Thixotropic	<b>Gels</b>	7000	Aveeno
	Silicone	Viscoelastic	<b>Thick</b>	8000	Smooth-on Eco-flex 00-50, RTP, Sampled over time;
	Grape Jam	Dilatant	<b>Slurries</b>	8500	Great Value
	Mayonnaise	Pseudoplastic	<b>Gels</b>	15000	Kraft
	Banana Pudding	Bingham Plastic	<b>Pastes</b>	30000	Bakery fresh banana pudding from local grocery store
	Hot Fudge	Bingham Plastic	<b>Pastes</b>	36000	Smucker
	Cooked Oatmeal	Dilatant	<b>Slurries</b>	100000	Quaker; 1:2 oatmeal to water; microwave for 5–10 minutes.
	Peanut Butter	Pseudoplastic	<b>Pastes</b>	250000	Good & Gather
	Spent Coffee Ground	Thixotropic	<b>Slurries</b>	-	Biofilament recipe [57] with Cafe Buetele spent coffee grounds
	Manufacturer's Clay Slip	Thixotropic	<b>Slurries</b>	-	Laquana Clay Company (S2459)
	Corn Starch (50%wt)	Pseudoplastic	<b>Pastes</b>	-	Kroger
	Alcohol	Bingham Plastic	<b>Ink</b>	-	CVS
	Fluid Acrylic	Bingham Plastic	<b>Ink</b>	-	Liquitex
	India Ink	Bingham Plastic	<b>Ink</b>	-	Bombay India Inks
	Pottery Plaster	Bingham Plastic	<b>Slurries</b>	-	AMACO Pottery Plaster

Figure 5: Materials Studied using RheoMap. Materials list was chosen based on the range of viscosity fluid materials. Note that all materials that are not labeled as Newtonian are non-Newtonian.

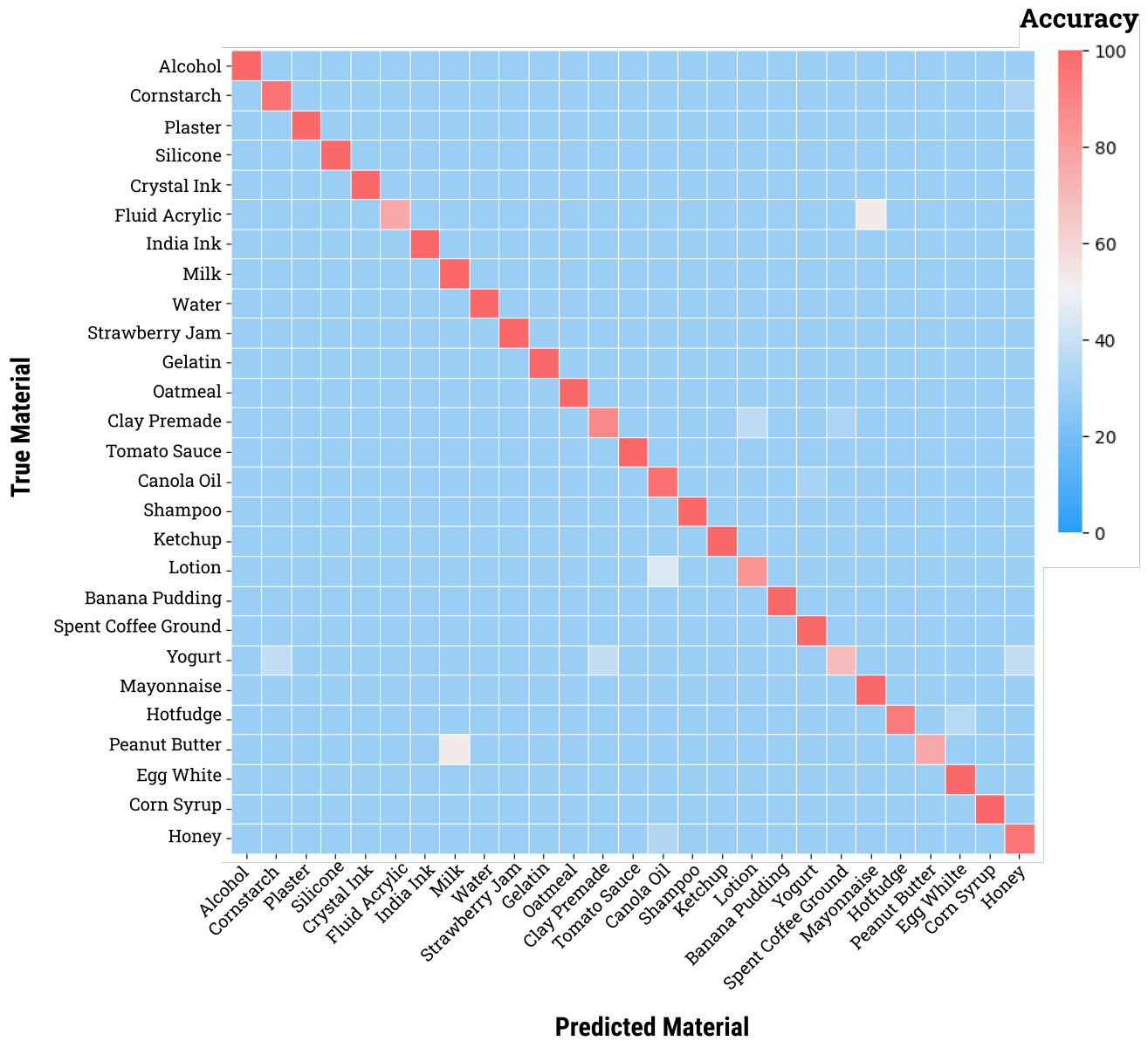


**Figure 6: Material Classification Confusion Matrix** The confusion matrix for 26 materials base on the Random Forest classifier to identify different materials on their features of REPs. Using a stratified 70-30 train-test split, the classifier achieved a weighted F1-score of 0.958, with 5-fold cross-validation yielding  $0.943 \pm 0.015$  (95% CI), demonstrating robust and consistent performance in identifying materials across diverse feature profiles.

50% of pump and motor power. Using water as the reference material, the system was calibrated, and cross-validation was performed on the extracted REP features for classification of the five fluid materials. The evaluation demonstrated an F1-weighted score of 74.69% for the small tube configuration and 88.18% for the reduced power configuration, indicating the effectiveness of the calibration technique in maintaining classification performance under different system conditions. These results suggest that our dataset of

26 materials can be extended to other system configurations while maintaining classification accuracy. The calibration process enables the REP signals to adapt to system changes with minimal error, supporting the scalability and generalization of our approach across different tube diameters, power levels, and motor configurations.

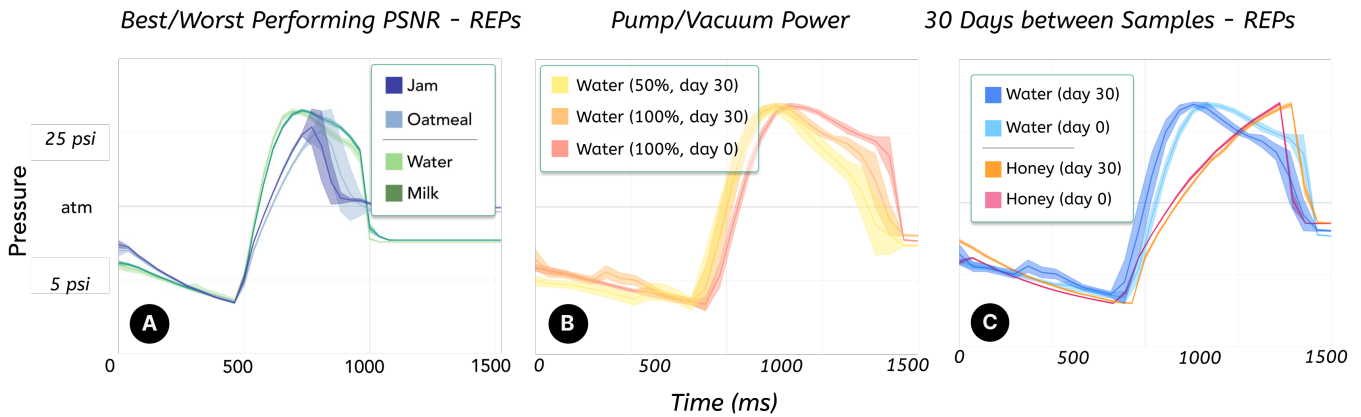


**Figure 7: Signal Quality Experiments** A) Signal Quality (PSNR) of REP - Water (41 dB), Milk (48 dB), Jam (31 dB) and Oatmeal (32 dB); shaded regions indicate the 68% confidence interval for the signal. B) Depicts the retraction-extrusion pulse patterns for water and honey, with data collected at two distinct times 30 days apart, to evaluate the system’s robustness. C) Illustrates the retraction-extrusion pulse space for water, highlighting variations over time and power.

## 5 RheoMap

To facilitate the navigation, interpretation, and manipulation of rheological behaviors, we employ latent space cartography to generate a “map” that projects the rheological sensor vectors onto a more interpretable 2D embedding space. We outline the process of creating these maps, present the resulting visualizations derived from multiple datasets, and demonstrate how to interpret the maps to uncover meaningful insights into rheological behavior.

### 5.1 Map Making Method

**Datasets.** The original **classification dataset** was used to generate the primary RheoMap, categorizing each sample by its material class ( $n=26$ ) and corresponding rheological class ( $m=6$ ).

**Mapping Technique.** The goal of map generation was to create an interpretable two-dimensional representation of fluid material behaviors that highlights clusters and patterns of rheological properties. To construct this embedding space, we tested several popular dimensionality reduction techniques, including Principal Component Analysis (PCA), Linear Discriminant Analysis (LDA), Uniform Manifold Approximation and Projection (UMAP), and t-distributed stochastic neighbor embedding (t-SNE). For each technique, we reduced the dimensionality of the classification dataset and visualized the cluster contours of each rheological class using a kernel density estimation (KDE) contour plot. Specifically, the KDE contour method [62] estimates the probability density function of the data and uses Gaussian kernels to smooth the distribution and creates a continuous probability surface. Contour lines represent regions of equal probability density, effectively visualizing the spatial distribution and overlap of each rheological class in the latent space. The following metrics were used to assess cartographic utility of the dimensionality reduction techniques:

- (1) *RheoClass and MatClass Preservation* was used to measure how effectively the reduced-dimensional representation maintains the grouping of rheological classes or material classes. This metric is calculated by evaluating the consistency of

corresponding class labels among the  $k$ -nearest neighbors in the reduced space. A higher score indicates that points belonging to the same class remain closely grouped.

- (2) *Spearman’s Rank Correlation* evaluated the monotonic relationship between pairwise distances in the high-dimensional and reduced spaces. This metric computes the correlation between ranked distances in both spaces, with higher values indicating that the relative ordering of distances is better preserved.
- (3) *Separation Distance* evaluated the degree of separation between clusters in the reduced space by calculating the mean pairwise distance between points from different classes. This mean inter-cluster distance is normalized by the maximum possible distance in the dataset. Higher separation distances reflect greater spatial segregation of clusters, reducing overlap and enhancing clarity between distinct classes.
- (4) *Cluster Compactness* measured the density of clusters in the reduced space by evaluating how tightly points within each rheological class are grouped. This is calculated by determining the average distance of points in each class to the class center, normalized by the number of points and the maximum pairwise distance in the dataset. Lower compactness scores indicate more dispersed clusters, while higher scores reflect tighter, more cohesive clusters, which are desirable for better interpretability.

The results for each dimensionality reduction methods are depicted in Figure 8). For RheoClass Preservation and MatClass Preservation, t-SNE achieves the highest scores (0.730 and 0.612, respectively) with comparable results from UMAP. As expected, the Spearman’s Rank Correlation is best preserved by PCA (0.963), however t-SNE was able to preserve distance relationships better than the other methods (0.796). For Separation Distance, t-SNE (0.426) and UMAP (0.423) effectively segregate clusters, outperforming PCA and LDA. In Cluster Compactness, t-SNE achieves the densest clusters (0.188), followed by UMAP. Overall, t-SNE was found to be the most effective for clustering and preserving global and local

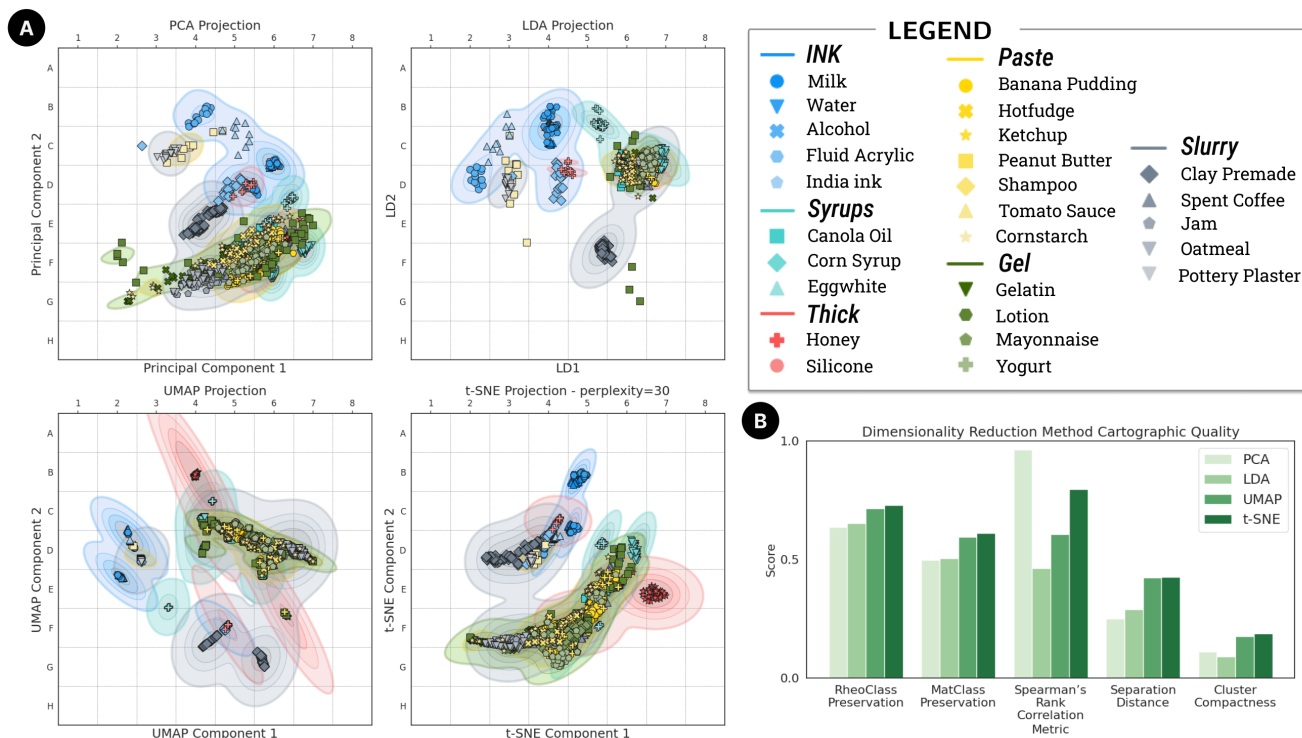


**Figure 8: Rheological Embedded Map A) Resulting embedding spaces from dimensionality reduction techniques Principal Component Analysis (PCA), Linear Discriminant Analysis (LDA), Uniform Manifold Approximation and Projection (UMAP), and t-distributed stochastic neighbor embedding (t-SNE); B) Performance of each embedding space as a cartographic map.**

relationships. It is used for all subsequent RheoMaps developed in this work.

*Map Rendering.* Murray et al. spatial design principles [40] were applied to improve the map's sensemaking qualities; the resulting t-SNE RheoMap is displayed in Figure 8. To create a sense of **place**, or recognizable and memorable spaces that users can easily identify and orient themselves, we first centered the embedding around the origin point. A **grid-based coordinate system**, akin to classic maps, were used to better reference and localize areas on the map. We also enabled the **zoom in functionality** that would preserve the reference grid system. Next, we applied reference materials as **landmarks**, using known fluids with well-known properties as anchor points on the map. We enabled the map to toggle between showing materials as points (centroid of the cluster), or as **neighborhoods** (contours that captures all members of the cluster). Each rheological classes were assigned a unique hue based on the closest **semiotic connection** (e.g., ink → blue ink; gel → translucent green) that also distinguished it from the other classes. Each material of a rheological classes was assigned a unique marker and color within the hue family. To create **waypoints** or marks that help users understand where they are, where they have been, and where they can go next, we plotted **routes** (lines with colored segments) for samples that had ordinal relationships (e.g., samples of silicone at different curing times).

## 5.2 Newtonian versus Non-Newtonian

The most prominent distinction in rheological types is associated with Newton's Law of Viscosity. Newtonian (N) materials, like water, have a constant viscosity regardless of the applied shear rate, meaning their resistance to flow remains unchanged whether stirred slowly or quickly. In contrast, Non-Newtonian (NN) materials change viscosity based on the force or speed applied. Depending on the type, these fluids can thin out, thicken, or exhibit a combination of behaviors, such as honey that becomes less viscous when stirred faster or cornstarch-water mixtures that thicken upon quick agitation.

We evaluated the ability of RheoMap for mapping different fluid materials in rheological embedding space, including Newtonian fluids (e.g., water, milk, india inks) ( $m=5, n=22$ ) and NN fluids (e.g., honey, ketchup, cornstarch, pottery plaster) ( $m=21, n=210$ ). As shown in Figure 9, both rheological classes occupy distinct regions of the RheoMap. Newtonian fluids such as water, milk, and canola oil span the B5:D5 column. In contrast, NN fluids exhibited two isolated band-shaped clusters: a smaller D-band and a larger F-band.

The small D-band, spanning D2:D4 notably overlapped with the Newtonian region, which was expected since these fluids are suspended in water, such as pre-made clay, pottery plaster, and cornstarch. The larger F-band of NN fluids, extends from F2:F4 and moved up to E5:D6. Similar to Newtonian behavior, the less viscous fluids are localized in the upper region of the band (D6), such as

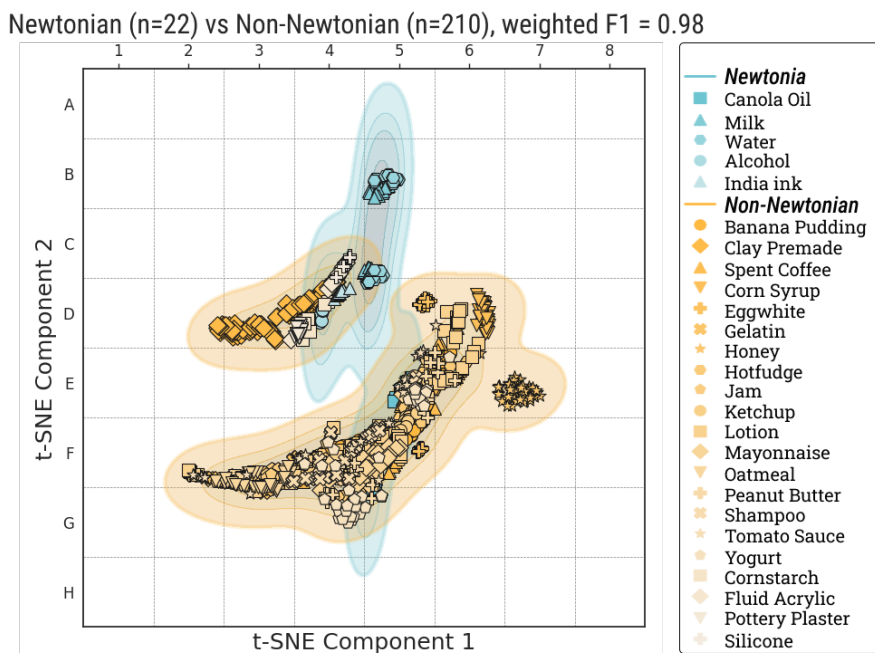


**Figure 9: Newtonian versus Non-Newtonian RheoMap.** The map of Newtonian (e.g., water, milk, india inks;  $m=5$ ;  $n=22$ ) and Non-Newtonian fluids (e.g., honey, ketchup, cornstarch, pottery plaster;  $m=21$ ;  $n=210$ )

egg white, corn syrup, and lotion. Notably, honey formed a distinct cluster in E7, positioned close to other NN fluids, likely due to its unique ability to mimic Newtonian behavior at the measured temperature, while still exhibiting traits that set it apart, such as its lack of particulate structures commonly found in other NN fluids like ketchup or mayonnaise. These characteristics reflect honey’s homogeneous molecular structure and sensitivity to external forces, distinguishing it within the broader group of complex fluids. The RheoMap is effective in distinguishing between Newtonian and NN fluids from the t-SNE coordinates alone – a decision tree classifier, trained on t-SNE-transformed data, achieved a mean weighted F1 score of 0.98 using stratified k-fold cross-validation ( $k=5$ ).

### 5.3 Viscosity

Viscosity is one of the most widely studied and commonly used rheological properties. To examine how effectively RheoMap discerns viscosity, we clustered materials into three distinct rheological classes based on their viscosity: inks (e.g., water, milk, alcohol;  $m=5$ ), syrups (e.g., corn syrup, egg white;  $m=3$ ), and thick substances (e.g., honey, silicone;  $m=2$ ). These materials were selected from majority from food-materials based on their well know viscosity values from food and materials science.

From Figure 10, the three sets of materials were distinctly represented. Ink-like materials were primarily located in the higher region, spanning B5: C5 and D4, reflecting their low viscosity properties and Newtonian behavior. Syrup-like materials (corn syrup and canola oil) were more distributed in D5: D6 and E5, corresponding to their medium viscosity values. Egg white was concentrated in E5 and G4, indicating its noisy signals, as egg white could create bubbles by the movement forces of RheoMap. Notably, honey and

silicone are located in the lower region, with honey at E6 and F5 and small amounts of silicone at C4, demonstrating their higher viscosity values. Additionally, these two materials exhibit Non-Newtonian behavior, not due to changes in viscosity from shear-force but rather from temperature and time factors. These behaviors may require further study and improvements in future systems. However, RheoMap demonstrated a clear distinction among the three types of materials—ink, syrup, and thick-like—corresponding to their respective increasing viscosity; more generally, these findings indicate that the A-H axis (t-SNE component 2) can be interpreted as encoding viscosity.

### 5.4 Gels and Pastes

Non-Newtonian (NN) materials are further distinguished by their behaviors over time. Time-dependent NNs (TD-NNs) exhibit a change in viscosity that evolves over time, whereas time-independent NNs (TI-NNs) depend only on the applied shear stress. Many modern paints are *thixotropic*, similar to pastes, meaning they become less viscous when stirred or shaken and return to their original, thicker state when at rest. When painting a wall for example, this allows the paint to rolled on and easily spread, but thickens once left to dry (over a period of time) preventing unsightly drips. In contrast, time-independent NNs, such as (*Bingham plastic*), as we categorized as gels, behave differently (gelatin and silicone). They require a certain force to flow out of a container, but revert to their original viscosity once the force is removed (yield stress behavior).

Using RheoMap, we visualized gels (e.g., gelatin, lotion, yogurt;  $m=4$ ;  $n=113$ ) and pastes (e.g., ketchup, shampoo;  $m=7$ ;  $n=137$ ) in the rheological embedding space. The t-SNE analysis revealed a shared cluster encompassing both gel-like and paste-like materials, with

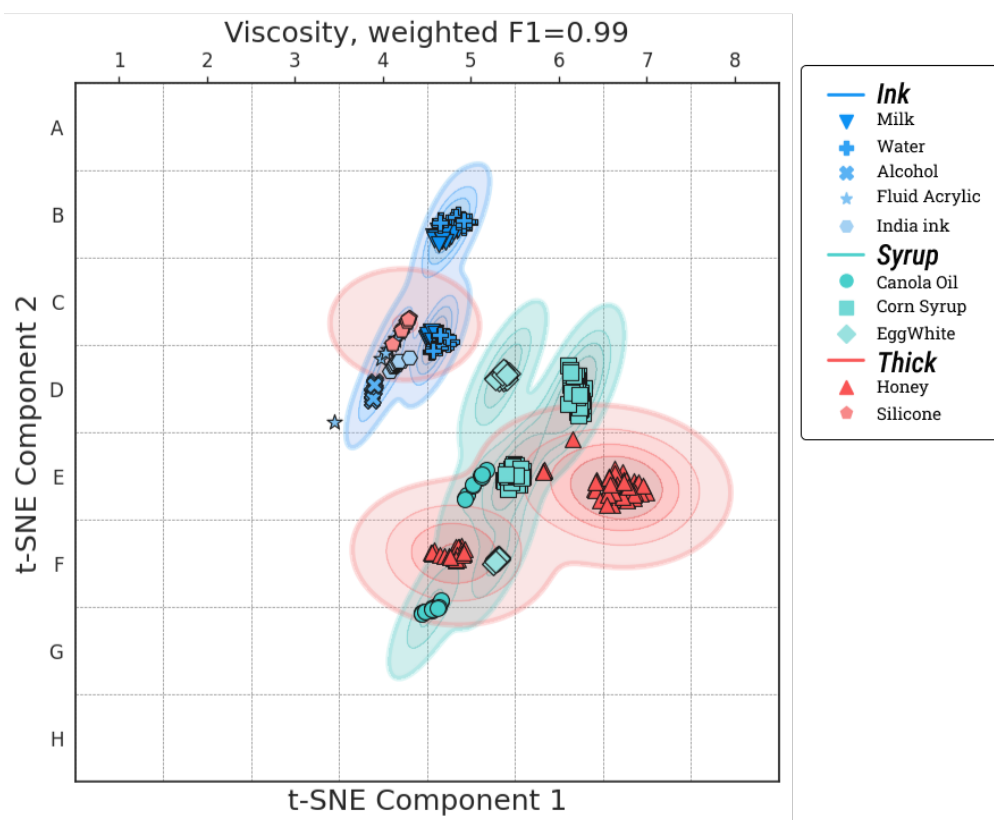


**Figure 10: Viscosity RheoMap** The map of materials categorized by viscosity, ranging from inks (e.g., water, milk, India ink;  $m=5$ ) to syrups (e.g., canola oil, corn syrup, egg white;  $m=3$ ) to thick materials (e.g., honey, silicone;  $m=2$ ). A decision tree classifier, trained on t-SNE-transformed data, achieved a mean weighted F1 score of 0.99 using stratified k-fold cross-validation ( $k=5$ ).

each material type occupying distinct locations within the cluster (Figure 11).

We observed that paste-like materials are located in the outer contour of the rheological embedding, characterized by shear-thinning and solid-like behavior. Variations in particle concentration, structure, and flow resistance within this group resulted in a slight spread across the F2:F5 and F5:D6 bands. In contrast, gel-like materials cluster tightly within the inner contour, reflecting their viscoelastic properties. These materials demonstrate a balance of liquid-like flow and solid-like deformation depending on applied force conditions.

The tight clustering of *gel-like materials* around F4 suggests a structured network that traps liquid, maintaining firmness until disturbed. For example, gelatin retains its form until a force disrupts its network. Gel-like materials often behave as Bingham plastics, requiring a yield stress to initiate flow, and may exhibit thixotropy—viscosity decreases under shear and gradually recovers when shear is removed. This time-dependent behavior is exemplified by lotion, which appears firm at rest, flows under shear (e.g., rubbing on skin), and recovers viscosity when the shear ceases.

In contrast, *paste-like materials*, while similarly solid-like, exhibit time-independent behavior. Their viscosity decreases under applied shear but recovers immediately once the stress is removed. These

distinctions place paste-like materials in the outer contour of the embedding.

Cornstarch presented an interesting outlier, occupying the upper region of D4. Its behavior depends significantly on the ratio of cornstarch to water, allowing it to transition between gel-like and paste-like states. In this study, a 1:1 ratio resulted in a thick fluid that primarily exhibited paste-like behavior but also shared characteristics with syrup-like or slurry-like materials.

Despite these nuanced behaviors, our approach achieved an F1-weighted score of up to 88% (t-SNE decision tree;  $r=2$ ; stratified k-fold cross-validation;  $k=5$ ), demonstrating the effectiveness of RheoMap in distinguishing between gel-like and paste-like materials. This differentiation highlights the capability of the embedding space to capture both shared and unique rheological properties of complex fluids.

## 5.5 Particle-Suspension (Slurries)

Another important consideration in the rheological characteristics of fluids is particle size and the uniformity of the mixture, which distinguishes fine particle slurries and large chunky particle slurries. Slurries are generally NN fluids, where viscosity decreases as shear stress increases, and consist of solid particles suspended in a

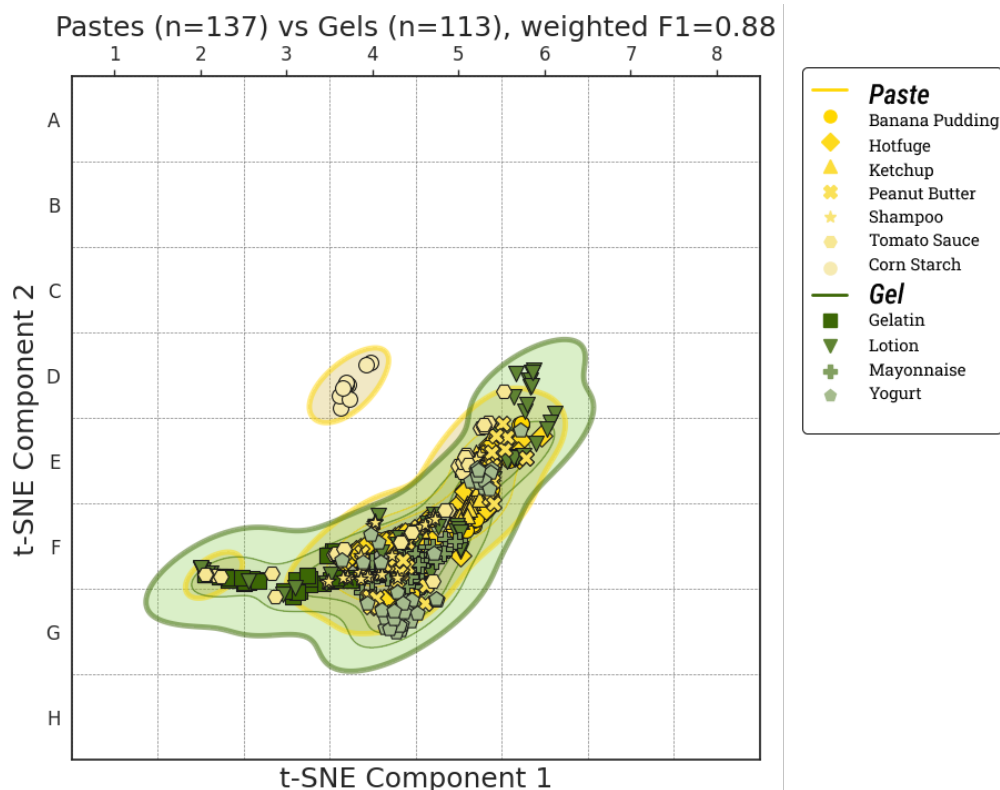


**Figure 11: Gels versus Pastes.** The t-SNE rheological embedded area of gels (e.g., gelatin, lotion, yogurt;  $m=4$ ;  $n=113$ ) and pastes fluid materials (e.g., ketchup, shampoo;  $m=7$ ;  $n=137$ ). A decision tree classifier, trained on t-SNE-transformed data, achieved a mean weighted F1 score of 0.88 using stratified k-fold cross-validation ( $k=5$ ).

non-uniform liquid medium. The size and concentration of these suspended particles significantly influence flow behavior, altering the viscous response and shear stress characteristics of the mixture.

Figure 12 illustrates distinct clusters of slurry types, categorized based on their viscous medium and particle size. For example, fine particle slurries (e.g., clay, pottery plaster;  $m=4$ ,  $n=210$ ), formed a tight cluster in the D3:D4 region, reflecting their rheological properties as small-particle, low-viscosity, water-based mixtures. In contrast, chunk particle slurries (e.g., tomato sauce and peanut butter;  $m=2$ ;  $n=112$ ) clustered in the lower right region (E5 and F4), indicative of higher viscosity and larger particle sizes. Both clusters exhibited shear-thinning behavior, a hallmark of NN fluids. Notably, tomato sauce and peanut butter exhibited some overlap within the F-band, likely due to noisy signals arising from sampling different regions of the non-homogeneous tomato sauce. This highlights an opportunity to enhance the REP signal by incorporating feature fusion – extracting and synthesizing features over multiple samples – to better capture rheological qualities that differ in heterogeneous materials.

In contrast, large chunky particle slurries primarily clustered in the lower region (F3:F4), reflecting their higher viscosity, larger particles, and chunkiness, which made them clearly distinguishable from other materials. Generally, an increase in particle size in fluids correlates with higher viscosity—a trend that RheoMap

effectively identified, achieving a weighted F1 score of 95% (t-SNE decision tree;  $r=2$ ; stratified k-fold cross-validation;  $k=5$ ). However, challenges arise when particle size changes while viscosity remains constant or in extreme cases involving micro- or larger particles. Such variations can produce complex fluid behaviors that test the system's limits. Additionally, particle size detection in RheoMap is constrained by the dimensions of the tube and the system's pump power. Addressing these limitations may require future iterations with stronger pumps and larger tubes. More significantly, analyzing complex fluids, particularly those involving micro- to nanoscale particles, will necessitate further intensive study and advanced techniques.

## 5.6 Concentration: Corn Syrup-Water

Concentration is a critical property to measure because it can influence a substance's various physical and chemical characteristics.

A **concentration dataset** of corn syrup-water solutions, comprising 586 samples with corn syrup content ranging from 10% to 100% by mass, was developed. Corn syrup was chosen due to its widespread use as a viscosity benchmark. This dataset was used to create a **specialized RheoMap**, applying t-SNE embedding exclusively on the concentration dataset, to enable tracking of fluid composition. This approach was designed to capture and highlight

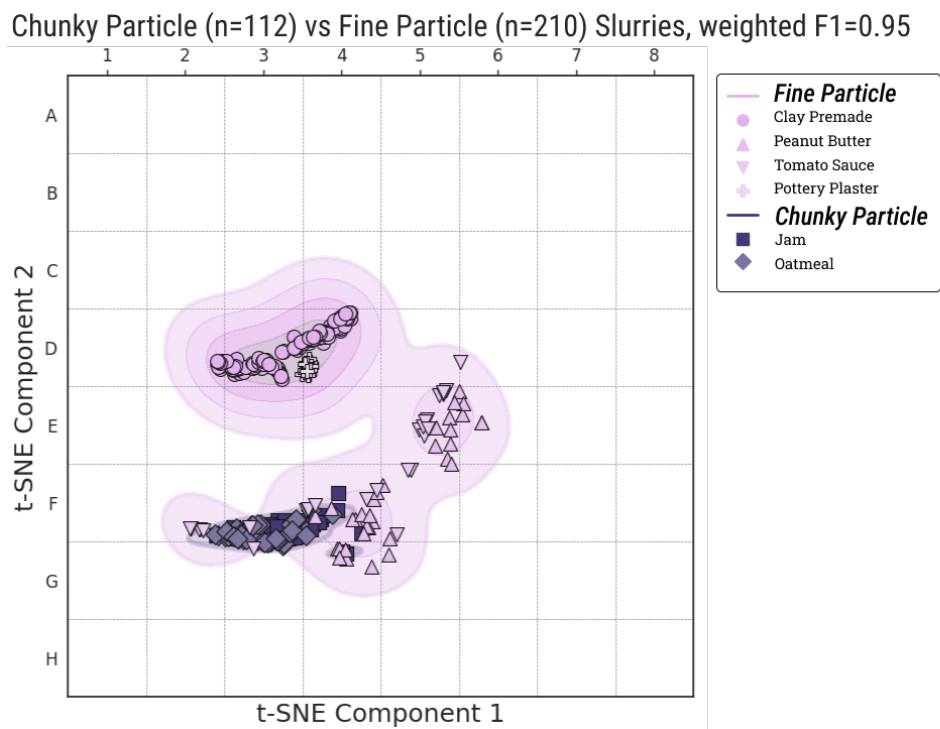


**Figure 12: Particle-Suspension RheoMap.** The rheological embedded area of slurries (heterogeneous) and non-slurries (homogenous) fluids based on two group: slurries (eg. tomato sauce, industrial slip casting clay, peanut butter;  $m=4$ ;  $n=210$ ) and non-slurries (jam and oatmeal;  $m=2$ ;  $n=112$ )

more minute changes in rheological properties across varying concentrations.

In this experiment, the solute (corn syrup) and the solvent (water) exhibited markedly different rheological profiles (NN and Newtonian, respectively). As established in our rheology experiments, this distinction is prominently captured by the RheoMap (Figure 9). We anticipate that the sensitivity of the retraction-extrusion pulses might be affected if the components of mixtures or solutions exhibit similar rheological characteristics (e.g., Newtonian - Newtonian solutions). The concentration route on the RheoMap (Figure 13A) illustrates the progression of corn syrup concentration, with lower concentrations mapped to higher regions, starting from B5 moving down to C-band as the corn syrup ratio increases. Higher concentrations shifted downward into F-band to G-band, ultimately ending at F6. The clear separation of regions reflects the transition from water-like (Newtonian) behavior at lower ratios to thicker, non-Newtonian behavior at higher corn syrup ratios. This sensitivity to rheological changes allows for an accurate representation of viscosity as a function of concentration and provides predictive capability in understanding rheological behavior. understanding the thresholds for achieving equivalent rheological behaviors (e.g., how much water to add before the material no longer behaves as a paste).

Due to the more complex spatial clusters on the t-SNE RheoMap, we trained a decision tree classifier on the LDA dimensionality-reduced data (3 discriminants, 97.76% variance explained) in contrast to prior t-SNE classifiers; the classifier was validated using k-fold cross-validation ( $k=10$ ). The classifier confusion matrices are depicted in Figure 13B. The model was able to distinguish between the ten concentration classes (each corresponding to differences in 10% concentration) with 83.33% accuracy. This indicates that RheoMap could provide a robust method for visualizing and predicting fluid concentrations, especially in situations where solutions change over time from evaporation.

## 5.7 Time Dynamic of Silicone and Gelatin

Fluids often exhibit changes in behavior and properties during the factor of time. These changes can result from alterations in their components, such as drying or due to chemical transformations like curing or setting. To understand the temporal sensitivity of REP, we examined the ability for the RheoMap system to distinguish such fluid shifts. Two **time-shift datasets** were collected to track dynamic material changes. For *silicone* (EcoFlex 00-50; 18 minute pot time), samples were taken every 3 seconds over a 50-minute cure at room temperature. The resulting dataset was grouped into the 6 stages of 8-minute intervals. For *gelatin* (unflavored), samples were taken hourly over a 2–3 hour setting period in a 40 °F (4.4 °C) refrigerator. These datasets were used to produce specialized

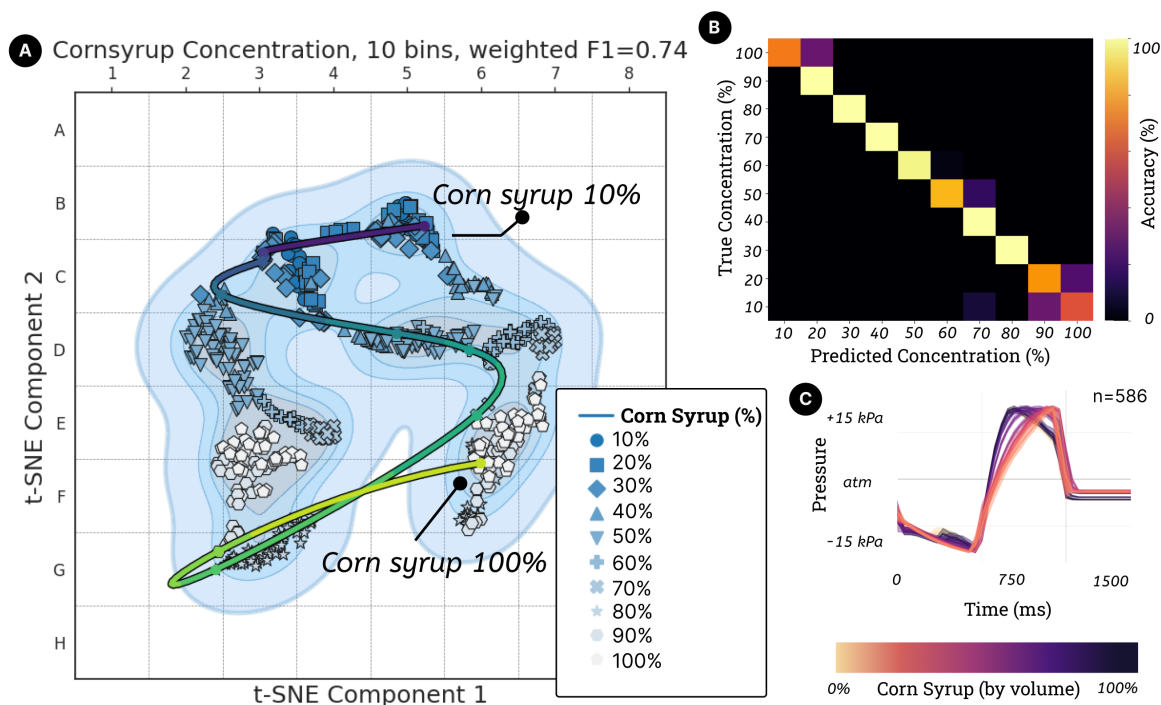


**Figure 13: Concentration Sensitivity.** A) The route map of corn syrup-water concentrations (by volume) with 10% increments in latent space; with starting at 10% and destination at 100% . B) The heatmap prediction with 83.33% accuracy. The confusion matrices illustrate true versus predicted concentration ratio (%) for classifications, C) retraction-extrusion pulses for collected samples.

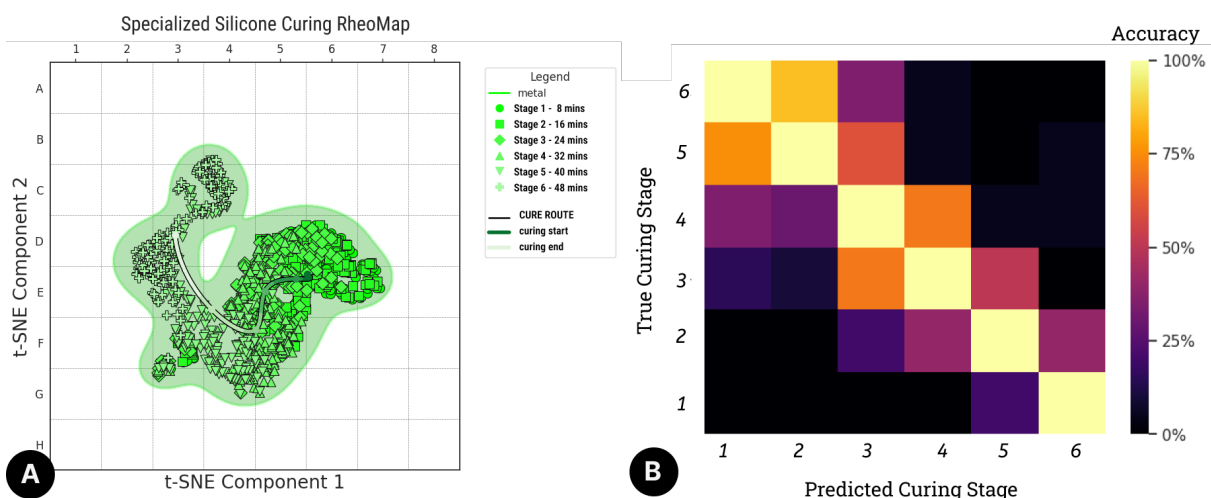


**Figure 14: RheoMap of Silicone Curing Sensitivity.** A) The route curing map of EcoFlex-50 silicone curing over time, divided into 6 incremental curing stages (8 minutes per stage) at a rate of 20 samples per minute in latent space. The process starts at 8 minutes and ends at 48 minutes with centroid data line. B) The heatmap predicts the curing time for each stage with 76.95%  $R^2$  accuracy. Note that EcoFlex-50 has an 18-minute pot time at room temperature. The confusion matrices illustrate true versus predicted classifications.

RheoMap that reveal material property transitions during curing and setting.

A **specialized RheoMap** was developed applying t-SNE embedding exclusively on the respective time-shift datasets to improve the granularity of the map; we added routes for the respective curing and setting processes.

The resulting RheoMap clusters curing stages into distinct temporally interconnected regions (Figure 14A). During the early curing stages (8, 16, and 24 minutes), the silicone clustered in the lower-left region from D5:D6 and E5:E7, exhibiting gel-like behavior with lower viscosity and yield stress, with the curing route (centroid datapoints) moving in E6:E5. This is expected behavior of silicone where slowly curing in beginning, soft and flowable under applied force but firms up when undisturbed (gels behavior). The later stages (32, 40, and 48 minutes) appeared in the upper leftward, suggests paste-like behavior, and moving rapidly from F4:E4 and end at D3:C4; indicates an increase in viscosity and curing rates. This is reflective of silicone curing faster during later cross-linking stages. Since the curing rate can be influenced by environmental factors (temperature, humidity, etc.), this presents a potential improvement area for RheoMap to reveal factors like temperature or humidity through the curing rate, enabling customized curing route maps for silicone based on different environments.

Also, we trained a decision tree classifier on the LDA dimensionality reduced data (3 discriminants, 97.76% variance explained; k-fold cross-validation; k=10) to classify the curing stage of silicone. The classifier performed with 54.62% accuracy. The confusion matrix indicates that adjacent stages account for the bulk of misclassification errors (Figure 14B). A regression model trained on the curing time of silicone achieved an  $R^2$  score of 76.95%. While not at the level of a scientific instrument, the REP pulses demonstrate enough granularity to achieve high-level characterization of curing stages.

For gelatin, we tracked four different curing times in 1-hour increments. In Figure 15 revealed transitions from gel-like to paste-like behavior, moving from lower region E7 to higher regions D4 in the map. However, unlike silicone, which was sampled continuously, gelatin indicates that the setting process is largely concentrated to the first hour. Despite this, the decision tree classifier on gelatin setting stage achieved a score of an F1-weighted score of 74% (r=3; stratified k-fold cross-validation; k=5). The map and confusion matrix (Figure 15 show that overlapping clusters and misclassification occurred when the gelatin was already set, still indicating a material state changes. These findings indicate that RheoMap can still function to detect state changes when not continuously sampling.

## 6 Exemplars

Exemplars serve as powerful tools to contextualize the diverse applications of a system, showcasing its potential in novel and innovative ways [23]. To motivate the utility of RheoMap within the HCI community, we describe a series of exemplars through a vignettes to illustrate the real-world use cases that can leverage RheoMaps.

### 6.1 Localization

New smart materials often need to be adapted for different applications. By displaying *landmarks* representing functional referents (e.g., gels, pastes, inks) on the map, makers can see how close their unknown material is to these established categories. Moreover, users often need a starting point to locate where they are and orientation in the embedded space. This where our tool could help as localization and navigation fluids materials through different type of fluids in rheological embedded space.

For instance, we analyzed a sample of Liquid Crystal (LC) material (SFSX) that had been in storage for nearly a year, raising questions about possible degradation in its material properties or its position in the embedded space relative to other fluids, as no one remembered its characteristics anymore. As a paint medium, the behavior of LC is largely determined by its binder – the component that enables it to be worked and applied in specific ways.

Our lab environment revealed potential relatives: a vial of india ink, a bottle of fluid medium, a jar of screen-printing paint, and a tube of heavy body acrylic paint. By finding the closest material relative, the RheoMap can be used to determine the types of tools and techniques developed by relative material practices to handle, coerce, and co-create with similar materials. On the RheoMap, we projected potential relatives as *landmarks*. We then projected a sample of the liquid crystal.

16).

Experimentally, we tested small amounts of LC using our sensing system to collect samples and map them on the RheoMap. We discovered that LC was centered in C4 (Figure 16), similar to fluid acrylic paint, and positioned higher compared to ink in D4. The LC was also distanced from the region of water (B5:E5) and alcohol in lower D4, clearly highlighting differences in fluid characteristics, as LC was thicker like thick or syrup-like; also more complex compared to water, alcohol, and inks. Notably, screen printing ink and heavy acrylic were thicker than all the other materials, shifting to D3, indicating their high viscosity. This also suggests that adding rheological modifiers such as CMC, xanthan gum, or cornstarch would shift the LC to these regions, providing guidance for recipe or map navigation within the embedded latent space.

Through this experiment, we documented these as potential fluids material to aid in navigating the rheological space and achieving desired rheological behaviors. We found that RheoMap could support the testing, recording, and annotating recipes using various rheological modifiers (e.g., thickeners, stabilizers, wetting agents). This approach facilitated understanding whether LC could be piped from an inkjet head, dispersed through an atomizer, or manipulated with a palette knife. This further supported *material polymorphism*, allowing for greater flexibility in adapting materials into different forms to enhance their compatibility with a wider range of application techniques.

### 6.2 Rheofencing

To help makers monitor material consistency over time and ensure expected behavior, we introduce a geofencing-inspired interaction called *rheofencing*. By leveraging REP readings from an established reference or ground truth, RheoMaps can track whether materials

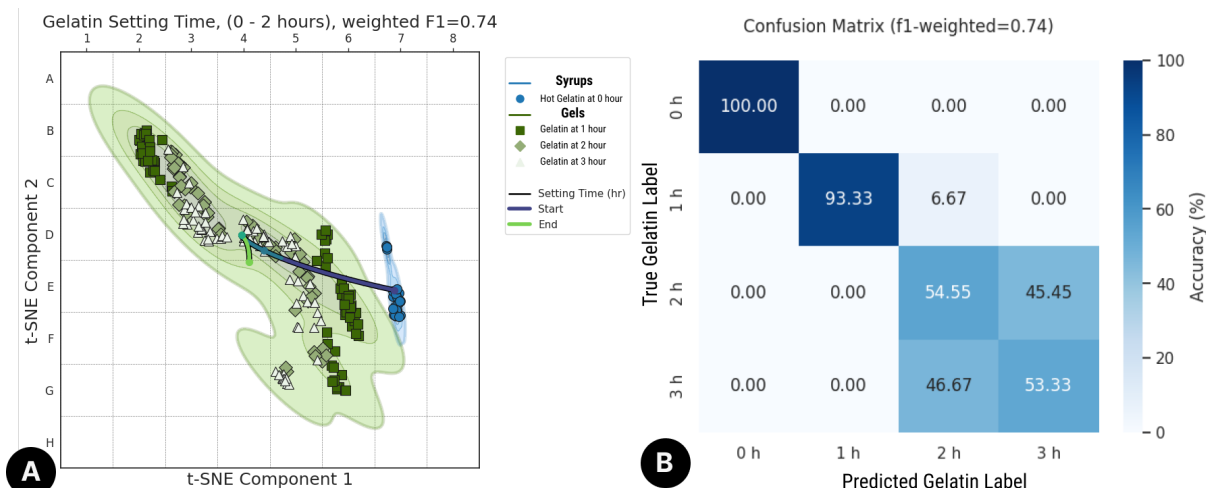


**Figure 15: RheoMap of Gelatin Curing Sensitivity.** A) The route curing map of gelatin curing over time, divided into 4 incremental curing stages (60 minutes per stage) in latent space. The map starts at initial mixing gelatin with hot water and ends at 3 hours later for curing. B) Details data of four gelatin curing stages with 0, 1 hour, 2 hour, and 3 hour respectively

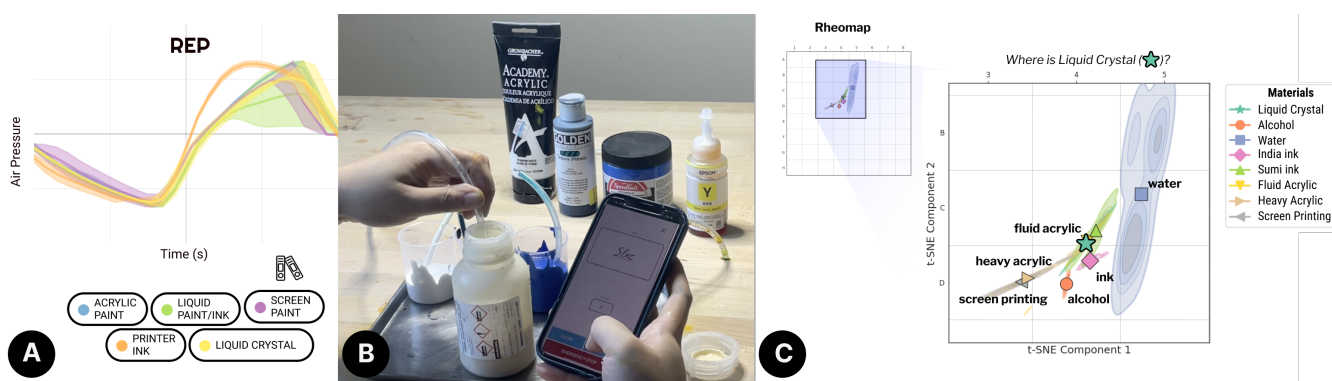


**Figure 16: Where in the RheoWorld is Liquid Crystal?** A Liquid Crystal material is compared against four common mediums: heavy body acrylic, fluid medium (used as a ink-paint), screen printing ink, and inkjet printer ink. A) The Retraction-Extrusion Plot shows the rheological profile of each viscous medium. B) Illustration of the experiment, collecting data from RheoMap to analyze and provide feedback through a phone app. C) Mapping Liquid Crystal in rheological embedded space indicates that it has similar rheological characteristics to inks and viscous materials. Based on collected samples through the app, RheoMap showed currently located material and suggest directions to reach the desired destination based on different fluid types, such as inks, gels, pastes, and slurries.

deviate during curing or setting processes. For instance, a common issue occurs when platinum-cure silicone is mixed with a wooden implement – the natural oils in the wood inhibit proper curing. Using reference readings from a successful cure, RheoMaps can assess whether a new curing routine aligns with the expected neighborhoods corresponding to different curing or setting stages. When monitoring a wood-mixed silicone, RheoMaps detected significant variations during curing stage 4. The contour maps for this stage showed reduced overlap and greater distinction compared to the reference silicone, indicating a deviation in the curing process (Figure 17).

Rheofencing enables early detection of deviations and integrates with end-user programming paradigms like trigger-action programming [58] to automate responses such as logging, SMS notifications, or alarms as materials transition through the map. For example, it can trigger alerts (e.g., "Curing Error") to warn makers of potential or ongoing material failures, enhancing temporal visibility and tracking of material interactions. Beyond monitoring, these virtual fences can also be employed to detect material failure more rapidly and adapt to challenging conditions, such as changes in temperature, humidity, or contamination.

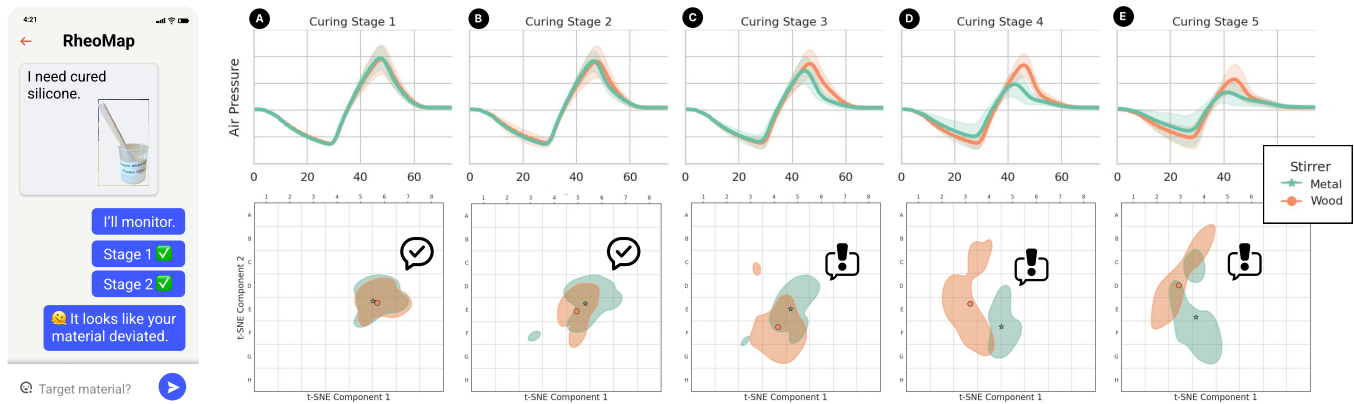


**Figure 17: Curing Silicone with Rheofences** Drawing from software debugging methods, we use the rheological embedding space to place makers in a rheological map that allows users to apply “geofences” for monitoring material workflows such as curing silicone. A) Showing message for monitoring wooden stirrer silicone curing overtime. B-E) Top row shows air pressure dynamics over time for curing stages. Bottom row displays t-SNE for the same curing stages, highlighting the distinctiveness of data patterns for each stirrer type.

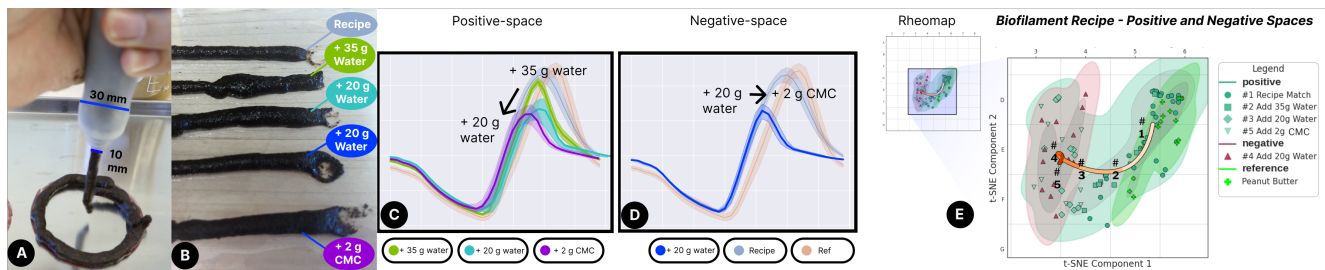


**Figure 18: Biofilament Neighborhood Mapping** A recipe for a biofilament from spent coffee grounds is replicated. A) A silicone piping pen was used to conduct an extrusion test to understand 3D printing behaviors. B) Extrusion tests for each SCG recipe based on recipe from Rivera et al. [48]; by adding 35g of water, an additional 40g of water (added in two 20g increments), and 2g of CMC, C) The REPs for each samples display in positive-space and negative space compare to reference: Rivera’s SCG recipe and peanut butter, D) Mapping SCG in rheological embedded space. Based on collected samples, RheoMap showed currently located material and neighborhood boundaries between positive and negative space . Contours on the map are thresholded to show density from 10% to 100%, highlighting the most populated parts of the space. Based on addition mixing material, RheoMap showed.

### 6.3 Neighborhood Mapping

RheoMaps present materials not as distinct points, but as neighborhoods. These neighborhoods, more generally, can be extended to represent **positive spaces** where a material meets desired characteristics, while **negative spaces** denote regions where materials fail to achieve these properties, resulting in unusable or unstable outcomes. A recipe, in this framework, can be seen as a single point within the positive space. However, deviations are often inevitable when following or modifying recipes, leading to uncertainty about whether a new formulation remains within the positive space or drifts into the negative space. This uncertainty presents challenges for customizing and optimizing material formulations.

We demonstrate how RheoMaps can chart a broader neighborhood of fluid materials, clarifying the boundaries between positive

and negative spaces. This enables flexibility in exploring and customizing recipes while improving replicability by identifying viable variations that maintain desired properties. For this study, we selected a biofilament recipe from Rivera et al. [48], which offers a sustainable alternative to thermoplastics by using readily available materials like spent coffee grounds (SCG) and viscosity modifiers (CMC, xanthan gum) to create a deposition-extrudable material with a “peanut-butter-like consistency.”

In this experiment, we replicated the original SCG biofilament recipe and produced four deviations by progressively adding water until the mixture failed, then reintroducing CMC to restore a paste-like consistency. Each variation was tested using manual extrusion tests with a 10 mm nozzle silicone injector syringe to assess extrusion behavior (Figure Figure 18A). The results were categorized into positive and negative spaces: positive spaces included formulations closer to the original recipe, exhibiting peanut

butter-like consistency and extrudability, while negative spaces represented formulations that deviated further, resulting in non-extrudable biofilaments.

Using RheoMap to map recipe variations (Figure 18C), we observed shifts in positive and negative spaces. Positive spaces moved leftward on the map, from E5 to E4, while negative spaces shifted rightward, remaining outside the positive zone. This highlighted RheoMap's ability to distinguish subtle changes in material behavior and assess extrudability limits. Through this exploration, RheoMap identified how far deviations from the original recipe could maintain biofilament extrudability and revealed the significant role of xanthan gum and CMC in the mixture. Fine-tuning the recipe showed that adding CMC unexpectedly reduced viscosity, demonstrating the value of the map's relational insights. Expanding RheoMaps to include more recipe variations could provide a reliable reference for extrudable materials, reducing costly and time-intensive tests. Additionally, RheoMaps could track material shifts over time (e.g., due to drying) and guide adjustments needed to restore variants to the positive space, supporting iterative material optimization.

## 7 Discussion

### 7.1 Map-Centered Exploration

Material development often relies on tracking variations, which frequently evolve from established recipes. For example, in creating a support bath for 3D-printed self-standing structures made from chocolate, jelly, alginate, and puff pastry, Yang et al. [64] first replicated an existing hydrogel recipe, adapting it for use with gelatin and creating a variant with carbopol. For that, it is important that users can track, follow, and annotate the recipe, allowing them to compare their progress more accurately and make adjustments if things go off track, making it easier to learn and experiment. We see that the RheoMap could allow makers to set a destination in the latent space representing a material reference point. When following a recipe, makers can monitor and compare their progress against the original recipe author's breakpoints, or readings taken at specific steps in the recipe. When designing or exploring a new material, makers can document their progress step-by-step through routes, or specify detours that split the developing recipe into two branches (version control) to facilitate systematic experimentation.

Moreover, the embedding sensor vector technique we used can be applied in various other fields beyond rheology. For instance, we employed air pressure as a means to gather data, but this approach could be extended to biomaterials, where parameters like pH, color, and turbidity are crucial. By embedding these measurements, one could generate maps that track changes across different phases of the cultivation or fabrication cycle. These maps would help highlight neighborhoods where biomaterials are either thriving or deteriorating, offering valuable insights into their health over time.

Additionally, the technique could be used to monitor and verify the state of biomaterials. For example, by identifying regions in the map where materials are dying, alerts could be sent directly to a phone, notifying users to take action.

For more dynamic, real-time feedback, the use of RheoMaps could provide visual and multi-modal feedback based on the map's data. One could generate spatial audio cues that allow users to

"listen" to their position within the map, helping them understand where they are in relation to the overall space. This method would enhance the usability and engagement of the embedding maps, offering an interactive way to monitor and analyze the materials in real time.

### 7.2 Comparison to Traditional Viscosity Methods

**Range:** Our experiments demonstrated the capacity for reliable and replicable experimentation but also enabled convenient monitoring and controlling of materials. RheoMap successfully captured REP for various materials, demonstrating its potential to distinguish between multi-material fluid mixtures from Newtonian to NN (0.5 cps to 250000 cps) which could hold promise for applications in fields such as HFI and inkjet printing. Khot et al. [21] described how printing chocolate requires care and attention to maintain the quality of food and its printable characteristics; under tempered chocolate could lead to watery prints. Lee et al. [24] also explored the internal structure of chocolate using 3D printing. Similarly, Khan et al. [20] noted that in addition to nozzle and surface, ink viscosity is one of the most important factors in multi-ink functional printing. The repeatability of our sensing method offers the ability to continually monitor and track the quality of such materials before and during the fabrication process.

**Material Limits:** Our method heavily relies on reference materials for our sensitivity to be effective and improve accuracy. Furthermore, the accuracy of MEMS pressure sensors and the effectiveness of air-pump power are also constrained. We found that our air pump did not have sufficient force to distinguish dilatants effectively. This leads to reduced accuracy and challenges in handling extreme materials, such as those with high viscosity or chunky consistency like peanut butter, hot fudge and other dilatant materials, which compared to traditional viscosity methods that typically employ cylinders or metal pistons. However, tube size and air pressure force is the most critical parameter to obtaining a clean and reliable signal.

**Rheological Tuning:** RheoMap device was effective in distinguishing between various concentrations of corn syrup and more generally to solutions where two different rheological types are present. Since water and oil (Newtonian) are often used as solvents, a wide variety of solutions fall under this purview. For the many HCI applications that leverage conductive ink (e.g., [65]), dialing in the flow of the material impacts its ability to be handled as a spray, paint, or 3D printed material.

Moreover, despite its success in differentiating between various concentrations of material, such as corn syrup solutions, our system demonstrated limitations when trying to distinguish between water (1 cPs) and other Newtonian materials like milk (3 cPs). This could be attributed to similarities in their behavior under identical environmental conditions or limitations within our current sensor and algorithm setup; coupling classic chromatography techniques could be used to help disambiguate similar rheologies. Although with our current experiments, the implementation of this technology presents certain challenges and requires further research, it has suggested effective with potential applications across various rheological substances and scenarios.

**Extendability and Portability:** Even though the rheological sensing demonstrates significant potential, it still requires custom hardware. We used off-the-shelf components to mitigate this; however, some of these components may become unavailable over time (e.g., Programmable Air). To improve extendability and portability, we introduced a calibration routine that uses water as a reference to adjust signals based on deviations in system configuration, such as motor power, air tube size, and sensor type, each demonstrating around 80% accuracy. This indicates that the calibration routine can facilitate the use of our material datasets to initialize other systems' RheoMap while supporting the creation of specialized RheoMap for more precise and granular applications.

**Extending the Sensing Routine:** We confirmed that [45] strategy of alternating between retraction and expulsion provides a rich rheological profile, however some rheological types remain out of reach. Distinguishing more complex rheological properties gels (time-dependent) and pastes (time-independence) in NN fluid requires incorporating non-linear forces into the RheoMap sensing routine; we view this additional distinction helping HCI researchers further tune the user-friendliness of materials. Similarly, difficulties were encountered when dealing with inks, gels, pastes, and slurries materials within Newtonina and NN. However, in reality, depending on the aspect that users measure—such as time, shear rate, or particle size; fluids can belong to either one or multiple categories.

Furthermore, fluid materials are mixed and the mixing technique, whether it be stirring, shaking, or using an ultrasonic homogenizer, are essential to creating new materials. Our classification model leveraged features gathered from an individual pulse, but when examining cycle level, such as PSNR, or from multi-site sampling shows potential increase the detection power. Our experiments with foam (whipped egg whites) showed distinct and more varied REP pulses (20% outlier rate), indicating a need to expand how REP features are encoded into machine learning models.

**Cost and Access:** We prioritized the use of off-the-shelf components such as the Programmable Air to encourage the adoption of REP sensing<sup>1</sup>. While this places the cost of the toolkit at \$200 USD, we see additional potential to make RheoMap low-power by using everyday syringes retrofitted with an air sensor to manually conduct the REP routine and further extend the ability to sense materials everywhere. Furthermore, as mentioned in the calibration section, our calibration routine is easy to use and accessible. Users could leverage our existing library in open source, which enables quick calibration using water as a reference material. We demonstrated how specialized rheology maps could be generated using a cycling routine to capture temporal data, offering a more comprehensive understanding of the material's rheological properties. This approach provides flexibility in both cost and precision, supporting a broad range of sensing applications.

### 7.3 Material Sensing in HCI

In ceramic and clay making, when formulating materials for applications like slip casting or for fluid-like substances such as silicone or carbon filament, it's imperative to understand their microstructure and particle properties. RheoMap has showcased its proficiency in

distinguishing between various slurries and non-slurries. However, the system encounters difficulties when trying to analysis strong and thick fluids or large particles. It also could not reveal further details characteristic of slurries and non-slurries, since some complex fluid could also Newtonian and NN, gels and pastes in both slurries and non-slurries type. Moreover, the small or larger microstructures, and even color, would be important fluid literacy, since RheoMap fail to detect. Moreover, to obtain accurate data during testing, stirring is often essential. This intricacy underscores a notable challenge for RheoMap which could be resolved by applying variable forces to the material versus when extruded.

The major challenges are in comprehending how fluid materials respond to various stresses, environmental factors, manipulation, time and costly; requires specialized equipment to conduct measurements. Generally, measuring viscosity is a common method for analyzing its properties like rheology, concentration, curing time, and extrudability. However, while exploring new fluid materials is often a slow and difficult process. The workflows vary widely, from fast-paced to day-long processes, adding another layer of complexity to manage fluid material behaviors. For example, printing edible films made from gelatin or starch required dissolving the material, reforming it as a gel, curing it for 5 minutes, and drying it for 12-18 hours [59]. Moreover, the dynamic qualities of materials often inhibit their adoption; a gelatin bath must be prepared in large batches to be worth the effort; even then, it can only be preserved for only 7 days [64]. Even though some practitioners have adopted scientific methods, these remain largely inaccessible. As a result, they lose the opportunity to innovate when working with "blackboxed" materials. With our system, we believe RheoMap could shine in this by annotating recipes and tutorials with waypoints, enabling a more accessible, open-source approach to fluid materials for replicating processes, testing, and debugging fluids. Furthermore, by integrating open-source resources, we envision enhanced collaboration through experimentation, innovation, and knowledge sharing, supported by DIY repositories and tutorials.

Lastly, material tuning, which involves adjusting a material's composition to produce a specific mixture, can significantly alter its rheological properties. While RheoMap shows promise in identifying and classifying a broad spectrum of materials to assist this process, it still faces challenges. For instance, distinguishing between closely similar materials like mayo and ketchup remains a hurdle. Also, during our tests on the behavior of foams using whipped egg white, distinct REPs were observed. However, these samples presented a 20% outlier rate. This result was expected due to the fluid-air composition of foams, causing them to behave differently from other fluids.

**Material Verification and Exploration Toolkits:** Fluid materials offer an extremely versatile design space, and consequently an even larger error space. We demonstrated RheoMap capacity to identify the curing state of materials such as silicone and gelatin. Silicone's curing time can be reduced by curing at a higher temperature, but its curing can also be inhibited by simply using a wooden implement to stir the mixture (platinum cure) [38]. When working with a new material, these unknowns can prohibit material exploration. The RheoMap could assist exploring new composites and fabrication techniques by verifying intermediate stages of these

<sup>1</sup>Open-source with provide software and firmware files for RheoMap: <https://github.com/The-Hybrid-Atelier/RheoMap>

materials' production and better document creative process with annotated prototypes. We viewed this freedom to play and experiment with material properties as a critical factor for enabling creativity in material practices.

**Smart Materials:** The materials sampled in our experiments were drawn from traditional material practices, however there is also the potential to use the REP method to characterize how smart materials respond to electro-magnetic, chemical, and mechanical stimulation. For instance, Jansen [18] found that magneto-rheological fluid (MR-fluid) can change viscosity when exposed to a magnetic field, but the change is invisible and can only be felt or observed. Haptic design tool-kits could leverage RheoMap to provide a profile to assist users in rapidly testing and tuning haptic expression by continually sampling (**cycle testing**) the viscosity of fluid while simultaneously being affected by different levels of magnetic stimulation.

## 7.4 Limitations

We are limited by our pump's power, preventing us from producing REP pulses for thicker fluids, like those used in cement and clay 3D printing. The current air pump shows power deficits, especially with larger tubes, resulting in noisy and unreliable pressure data. The system currently works only with small, predefined tubes and cannot operate with a check valve, which is crucial to prevent materials from entering the pump and electrical components. However, hydrophobic check valves, commonly used in medical devices, could provide a solution by venting gases while preventing liquid passage.

Our sensing method can sense material concentrations but is currently restricted to material versus water. Future improvements may include exploring alternative components, varying air tube dimensions, and regular calibration. Maintaining system robustness while protecting electronic components without affecting the REP signal remains a challenge. One possible way to minimize electrical components is by replacing the pneumatic pump with manual air controls, such as a syringe, to create a nearly passive system. Further enhancing durability may require integrating waterproof air pressure sensors or improving calibration detection.

## 8 Conclusion

RheoMap has demonstrated significant potential mapping and navigating a diverse range of fluid materials such as inks, gels, pastes and slurries in rheological embedded latent space. Leveraging a retraction-extrusion pulse approach with off-the-shelf pneumatic systems, our system minimizes material consumption and allows for quick-repeatable cycle testing. However, dealing with complex materials or substances with close similarities presents challenges. To address these, advancements in hardware and sensing routines are crucial, particularly in scenarios involving intricate microstructures and heterogeneous materials. RheoMap's ability to navigating between unique fluid types: inks, gels, pastes and slurries, as well as tracking fluid's concentration, time-shifting and extrudability. This properties has good implications for its practical use in many areas for monitoring and controlling, especially in digital fabrication and interaction design. By releasing RheoMap as an open-source

system, we aim to be as support tutorial tool-kits that allow access complex fluid materials and reveal materials literacy.

## Acknowledgments

We thank the reviewers for their insightful feedback, Ciara Sorrells for helping with ceramics and figures, and, importantly, our peers from The Hybrid Atelier at UTA for their invaluable support.

## References

- [1] Texture Analyzers. 2023. *Extrusion*. N/A. <https://www.textureanalyzers.com/extrusion>
- [2] Fiona Bell and Mirela Alistar. 2022. Designing with Alganyl: A Hands-on Exploration of Biodegradable Plastics. In *Proceedings of the Sixteenth International Conference on Tangible, Embedded, and Embodied Interaction* (Daejeon, Republic of Korea) (TEI '22). Association for Computing Machinery, New York, NY, USA, Article 56, 5 pages. doi:10.1145/3490149.3503669
- [3] Fiona Bell, Erin McClure, Camila Friedman-Gerlicz, Ruby Ta, and Leah Buechley. 2024. Shape-Changing Clay-Dough: Taking a Material-Oriented Approach to 3D Printing Ceramic Forms. In *Proceedings of the CHI Conference on Human Factors in Computing Systems* (Honolulu, HI, USA) (CHI '24). Association for Computing Machinery, New York, NY, USA, Article 864, 19 pages. doi:10.1145/3613904.3642246
- [4] Fiona Bell, Netta Ofer, Ethan Frier, Ella McQuaid, Hyelin Choi, and Mirela Alistar. 2022. Biomaterial Playground: Engaging with Bio-based Materiality. In *Extended Abstracts of the 2022 CHI Conference on Human Factors in Computing Systems* (New Orleans, LA, USA) (CHI EA '22). Association for Computing Machinery, New York, NY, USA, Article 171, 5 pages. doi:10.1145/3491101.3519875
- [5] Christopher M. Bishop. 2006. *Pattern Recognition and Machine Learning*. Springer, N/A.
- [6] Justin Chan, Ananditha Raghunath, Kelly E. Michaelsen, and Shyamnath Gollakota. 2022. Testing a Drop of Liquid Using Smartphone LiDAR. arXiv:2203.07567 [cs.CY]
- [7] Minsuk Chang, Leonore V. Guillain, Hyeungshik Jung, Vivian M. Hare, Juho Kim, and Maneesh Agrawala. 2018. RecipeScape: An Interactive Tool for Analyzing Cooking Instructions at Scale. In *Proceedings of the 2018 CHI Conference on Human Factors in Computing Systems* (Montreal QC, Canada) (CHI '18). Association for Computing Machinery, New York, NY, USA, 1–12. doi:10.1145/3173574.3174025
- [8] Wei Wei Chi and Daragh Byrne. 2020. Cultivating Material Knowledge: Experiments with a Low Cost Interface for 3D Texture Scanning. In *Proceedings of the 2020 ACM Designing Interactive Systems Conference* (Eindhoven, Netherlands) (DIS '20). Association for Computing Machinery, New York, NY, USA, 1089–1102. doi:10.1145/3357236.3395579
- [9] T.G. Chuah, H. Hairul Nisah, S.Y. Thomas Choong, N.L. Chin, and A.H. Nazimah Sheikh. 2007. Effects of temperature on viscosity of dodol (concoction). *Journal of Food Engineering* 80 (2007), 423–430. Issue 2. doi:10.1016/j.jfoodeng.2006.04.051
- [10] Rafael M. Digilov. 2011. Pressure-driven capillary viscometer: Fundamental challenges in transient flow viscometry. *Review of Scientific Instruments* 82, 12 (12 2011), 125111. doi:10.1063/1.3671572 arXiv:https://pubs.aip.org/aip/rsi/article-pdf/doi/10.1063/1.3671572/8827425/125111\_1\_online.pdf
- [11] Mustafa Doga Dogan, Steven Vidal Acevedo Colon, Varnika Sinha, Kaan Aksit, and Stefanie Mueller. 2021. SensiCut: Material-Aware Laser Cutting Using Speckle Sensing and Deep Learning. In *The 34th Annual ACM Symposium on User Interface Software and Technology* (Virtual Event, USA) (UIST '21). Association for Computing Machinery, New York, NY, USA, 24–38. doi:10.1145/3472749.3474733
- [12] Shreyosi Endow and Cesar Torres. 2023. Tacit Descriptions: Uncovering Ambiguity in Crowdsourced Descriptions of Motions and Materials. In *Proceedings of the 2023 ACM Designing Interactive Systems Conference* (Pittsburgh, PA, USA) (DIS '23). Association for Computing Machinery, New York, NY, USA, 2522–2536. doi:10.1145/3563657.3596048
- [13] Melanie Feinberg. 2017. Material Vision. In *Proceedings of the 2017 ACM Conference on Computer Supported Cooperative Work and Social Computing* (Portland, Oregon, USA) (CSCW '17). Association for Computing Machinery, New York, NY, USA, 604–617. doi:10.1145/2998181.2998204
- [14] Elisa Giacardi and Elvin Karana. 2015. Foundations of Materials Experience: An Approach for HCL. In *Proceedings of the 33rd Annual ACM Conference on Human Factors in Computing Systems* (Seoul, Republic of Korea) (CHI '15). Association for Computing Machinery, New York, NY, USA, 2447–2456. doi:10.1145/2702123.2702337
- [15] Honeywell. 201. *MicroPressure Board Mount Pressure Sensors Compact, High Accuracy, Compensated/Amplified*. Honeywell, Honeywell Sensing and Internet of Things, 9680 Old Baires Road Fort Mill, SC 29707. Available online: <https://cdn.sparkfun.com/assets/2/e/8/0/9/honeywell-mpr-datashet.pdf>.
- [16] T. Hoshino. 2020. Analysis of viscosity measurements obtained using the short back extrusion method. Part 1: Theory of short back extrusion in viscometry. *J*

- Texture Stud* 51 (2020), 201–213. <https://doi.org/10.1111/jtxs.12501>
- [17] Yongzhi Huang, Kaixin Chen, Yandao Huang, Lu Wang, and Kaishun Wu. 2021. Vi-Liquid: Unknown Liquid Identification with Your Smartphone Vibration. In *Proceedings of the 27th Annual International Conference on Mobile Computing and Networking* (New Orleans, Louisiana) (*MobiCom '21*). Association for Computing Machinery, New York, NY, USA, 174–187. doi:10.1145/3447993.3448621
- [18] Yvonne Jansen. 2010. Mudpad: Fluid Haptics for Multitouch Surfaces. In *CHI '10 Extended Abstracts on Human Factors in Computing Systems* (Atlanta, Georgia, USA) (*CHI EA '10*). Association for Computing Machinery, New York, NY, USA, 4351–4356. doi:10.1145/1753846.1754152
- [19] Hsin-Liu (Cindy) Kao, Miren Bamforth, David Kim, and Chris Schmandt. 2018. Skinmorph: Texture-Tunable on-Skin Interface through Thin, Programmable Gel. In *Proceedings of the 2018 ACM International Symposium on Wearable Computers* (Singapore, Singapore) (*ISWC '18*). Association for Computing Machinery, New York, NY, USA, 196–203. doi:10.1145/3267242.3267262
- [20] Arshad Khan, Joan Sol Roo, Tobias Kraus, and Jürgen Steimle. 2019. Soft Inkjet Circuits: Rapid Multi-Material Fabrication of Soft Circuits Using a Commodity Inkjet Printer. In *Proceedings of the 32nd Annual ACM Symposium on User Interface Software and Technology* (New Orleans, LA, USA) (*UIST '19*). Association for Computing Machinery, New York, NY, USA, 341–354. doi:10.1145/3332165.3347892
- [21] Rohit Ashok Khot, Deepthi Aggarwal, Ryan Pennings, Larissa Hjorth, and Florian 'Floyd' Mueller. 2017. EdiPulse: Investigating a Playful Approach to Self-Monitoring through 3D Printed Chocolate Treats. In *Proceedings of the 2017 CHI Conference on Human Factors in Computing Systems* (Denver, Colorado, USA) (*CHI '17*). Association for Computing Machinery, New York, NY, USA, 6593–6607. doi:10.1145/3025453.3025980
- [22] Matthew Lanaro, Mathilde R Desselte, and Maria A Woodruff. 2019. 3D printing chocolate: properties of formulations for extrusion, sintering, binding and ink jetting. In *Fundamentals of 3D food printing and applications*. Elsevier, N/A, 151–173.
- [23] David Ledo, Steven Houben, Jo Vermeulen, Nicolai Marquardt, Lora Oehlborg, and Saul Greenberg. 2018. Evaluation Strategies for HCI Toolkit Research. In *Proceedings of the 2018 CHI Conference on Human Factors in Computing Systems* (Montreal QC, Canada) (*CHI '18*). Association for Computing Machinery, New York, NY, USA, 1–17. doi:10.1145/3173574.3173610
- [24] Yujin Lee, Jee Bin Yim, Daye Kang, HyeonBeom Yi, and Daniel Saakes. 2019. Designing Internal Structure of Chocolate and Its Effect on Food Texture. In *Companion Publication of the 2019 on Designing Interactive Systems Conference 2019 Companion* (-conf-loc-, <city>San Diego</city>, <state>CA</state>, <country>USA</country>, </conf-loc>) (*DIS '19 Companion*). Association for Computing Machinery, New York, NY, USA, 231–235. doi:10.1145/3301019.3323896
- [25] Yumeng Liang, Anfu Zhou, Huanhuan Zhang, Xinzhe Wen, and Huadong Ma. 2021. FG-LiquidID: A Contact-Less Fine-Grained Liquid Identifier by Pushing the Limits of Millimeter-Wave Sensing. *Proc. ACM Interact. Mob. Wearable Ubiquitous Technol.* 5, 3, Article 116 (sep 2021), 27 pages. doi:10.1145/3478075
- [26] David Chuan-En Lin, Fabian Caba Heilbron, Joon-Young Lee, Oliver Wang, and Nikolas Martelaro. 2024. VideoMap: Supporting Video Exploration, Brainstorming, and Prototyping in the Latent Space. In *Proceedings of the 16th Conference on Creativity & Cognition* (Chicago, IL, USA). Association for Computing Machinery, New York, NY, USA, 311–327. doi:10.1145/3635636.3656192
- [27] Yang Liu, Eunice Jun, Qisheng Li, and Jeffrey Heer. 2019. Latent space cartography: Visual analysis of vector space embeddings. In *Computer graphics forum*, Vol. 38. Wiley Online Library, N/A, N/A, 67–78.
- [28] Qiuyu Lu, Lydia Yang, Aditi Maheshwari, Hengrong Ni, Tianyu Yu, Jianzhe Gu, Advait Wadhvani, Haiqing Xu, Andreea Danielescu, and Lining Yao. 2024. Guttation Sensor: Wearable Microfluidic Chip for Plant Condition Monitoring and Diagnosis. In *Extended Abstracts of the CHI Conference on Human Factors in Computing Systems* (Honolulu, HI, USA) (*CHI EA '24*). Association for Computing Machinery, New York, NY, USA, Article 183, 9 pages. doi:10.1145/3613905.3651087
- [29] Kent Lyons. 2024. Shape Cast: Automating 3D Design for Plaster Molds in Ceramic Slip Casting. In *Extended Abstracts of the 2024 CHI Conference on Human Factors in Computing Systems* (*CHI EA '24*). Association for Computing Machinery, New York, NY, USA, Article 287, 7 pages. doi:10.1145/3613905.3651020
- [30] C.W. Macosko. 1994. *Rheology: Principles, Measurements and Applications*. VCH Publishers, New York.
- [31] Mohammadamin Mahmoudabadbozchelou, Marco Caggioni, Setareh Shahsavari, William H. Hartt, George Em Karniadakis, and Safa Jamali. 2021. Data-driven physics-informed constitutive metamodeling of complex fluids: A multifidelity neural network (MFNN) framework. *Journal of Rheology* 65, 2 (03 2021), 179–198. doi:10.1122/8.0000138 arXiv:https://pubs.aip.org/sor/jor/article-pdf/65/2/179/12509804/179\_1\_online.pdf
- [32] Mohammadamin Mahmoudabadbozchelou and Safa Jamali. 2021. Rheology-Informed Neural Networks (RhINNs) for forward and inverse metamodeling of complex fluids. *Scientific Reports* 11, 1 (2021), 12015. doi:10.1038/s41598-021-91518-3
- [33] Mohammadamin Mahmoudabadbozchelou, Krutarth M. Kamani, Simon A. Rogers, and Safa Jamali. 2022. Digital rheometer twins: Learning the hidden rheology of complex fluids through rheology-informed graph neural networks. *Proceedings of the National Academy of Sciences* 119, 20 (2022), e2202234119. doi:10.1073/pnas.2202234119 arXiv:https://www.pnas.org/doi/pdf/10.1073/pnas.2202234119
- [34] Alex Mariakakis, Sifang Chen, Bichlien H. Nguyen, Kirsten Bray, Molly Blank, Jonathan Lester, Lauren Ryan, Paul Johns, Gonzalo Ramos, and Asta Roseway. 2020. EcoPatches: Maker-Friendly Chemical-Based UV Sensing. In *Proceedings of the 2020 ACM Designing Interactive Systems Conference* (-conf-loc-, <city>Eindhoven</city>, <country>Netherlands</country>, </conf-loc>) (*DIS '20*). Association for Computing Machinery, New York, NY, USA, 1983–1994. doi:10.1145/3357236.3395424
- [35] Mako Miyatake, Koya Narumi, Yuji Sekiya, and Yoshihiro Kawahara. 2021. Flower Jelly Printer: Slit Injection Printing for Parametrically Designed Flower Jelly. In *Proceedings of the 2021 CHI Conference on Human Factors in Computing Systems* (Yokohama, Japan) (*CHI '21*). Association for Computing Machinery, New York, NY, USA, Article 425, 10 pages. doi:10.1145/3411764.3445346
- [36] Hila Mor, Tianyu Yu, Ken Nakagaki, Benjamin Harvey Miller, Yichen Jia, and Hiroshi Ishii. 2020. Venous Materials: Towards Interactive Fluidic Mechanisms. In *Proceedings of the 2020 CHI Conference on Human Factors in Computing Systems* (Honolulu, HI, USA) (*CHI '20*). Association for Computing Machinery, New York, NY, USA, 1–14. doi:10.1145/3313831.3376129
- [37] Hedieh Moradi, Long N Nguyen, Quyen-Anh Valentina Nguyen, and Cesar Torres. 2022. Glaze Epochs: Understanding Lifelong Material Relationships within Ceramics Studios. In *Proceedings of the Sixteenth International Conference on Tangible, Embedded, and Embodied Interaction* (Daejeon, Republic of Korea) (*TEI '22*). Association for Computing Machinery, New York, NY, USA, Article 4, 13 pages. doi:10.1145/3490149.3501310
- [38] Hedieh Moradi and César Torres. 2020. Siloseam: A Morphogenetic Workflow for the Design and Fabrication of Inflatable Silicone Bladders. In *Proceedings of the 2020 ACM Designing Interactive Systems Conference* (Eindhoven, Netherlands) (*DIS '20*). Association for Computing Machinery, New York, NY, USA, 1995–2006. doi:10.1145/3357236.3395473
- [39] João Mouro, Rui Pinto, Paolo Paoletti, and Bruno Tiribilli. 2021. Microcantilever: Dynamical Response for Mass Sensing and Fluid Characterization. *Sensors* 21, 1 (2021), N/A. doi:10.3390/s21010115
- [40] JH Murray. 2011. *Inventing the Medium: Principles of Interaction Design as a Cultural Practice*. The MIT Press, N/A.
- [41] N/A. N/A. *Texture Analyzer*. N/A. <https://www.stablemicrosystems.com/N/A>.
- [42] Ali Nadernezhad and Jürgen Groll. 2022. Machine Learning Reveals a General Understanding of Printability in Formulations Based on Rheology Additives. *Advancing Science* 9, 29 (2022), 2202638. doi:10.1002/adv.202202638 arXiv:https://onlinelibrary.wiley.com/doi/pdf/10.1002/adv.202202638
- [43] Sigeru Omatu. 2013. Odor classification by neural networks. In *2013 IEEE 7th International Conference on Intelligent Data Acquisition and Advanced Computing Systems (IDAACS)*, Vol. 01. N/A, N/A, 309–314. doi:10.1109/IDAACS.2013.6662695
- [44] F. Pedregosa, G. Varoquaux, A. Gramfort, V. Michel, B. Thirion, O. Grisel, M. Blondel, P. Prettenhofer, R. Weiss, V. Dubourg, J. Vanderplas, A. Passos, D. Cournapeau, M. Brucher, M. Perrot, and E. Duchesnay. 2011. Scikit-learn: Machine Learning in Python. *Journal of Machine Learning Research* 12 (2011), 2825–2830.
- [45] Arnaud Perrot, Yannick Mélinge, Patrice Estellé, Damien Rangedard, and Christophe Lanos. 2011. The Back Extrusion Test as a Technique for Determining the Rheological and Tribological Behaviour of Yield Stress Fluids at Low Shear Rates. *Applied Rheology* 21, 5 (2011), 53642. <https://doi.org/10.3933/apprheol-21-53642>
- [46] Michael JD Powell. 1964. An efficient method for finding the minimum of a function of several variables without calculating derivatives. *The computer journal* 7, 2 (1964), 155–162.
- [47] Isabel PS Qamar, Rainer Groh, David Holman, and Anne Roudaut. 2018. HCI meets material science: A literature review of morphing materials for the design of shape-changing interfaces. In *Proceedings of the 2018 CHI Conference on Human Factors in Computing Systems*. N/A, N/A, 1–23.
- [48] Michael L. Rivera, S. Sandra Bae, and Scott E. Hudson. 2023. Designing a Sustainable Material for 3D Printing with Spent Coffee Grounds. In *Proceedings of the 2023 ACM Designing Interactive Systems Conference* (Pittsburgh, PA, USA) (*DIS '23*). Association for Computing Machinery, New York, NY, USA, 294–311. doi:10.1145/3563657.3595983
- [49] Michael L. Rivera, Jack Forman, Scott E. Hudson, and Lining Yao. 2020. Hydrogel-Textile Composites: Actuators for Shape-Changing Interfaces. In *Extended Abstracts of the 2020 CHI Conference on Human Factors in Computing Systems* (Honolulu, HI, USA) (*CHI EA '20*). Association for Computing Machinery, New York, NY, USA, 1–9. doi:10.1145/3334480.3382788
- [50] Munehiko Sato, Shigeo Yoshida, Alex Olwal, Boxin Shi, Atsushi Hiyama, Tomohiro Tanikawa, Michitaka Hirose, and Ramesh Raskar. 2015. SpecTrans: Versatile Material Classification for Interaction with Textureless, Specular and Transparent Surfaces. In *Proceedings of the 33rd Annual ACM Conference on Human Factors in Computing Systems* (Seoul, Republic of Korea) (*CHI '15*). Association for Computing Machinery, New York, NY, USA, 2191–2200. doi:10.1145/2702123.2702169

- [51] Amitabh Shrivastava. N/A. *Programmable Air*. N/A, N/A. <https://www.programmableair.com> N/A.
- [52] Thomas Smith, Simon J. Bowen, Bettina Nissen, Jonathan Hook, Arno Verhoeven, John Bowers, Peter Wright, and Patrick Olivier. 2015. Exploring Gesture Sonification to Support Reflective Craft Practice. In *Proceedings of the 33rd Annual ACM Conference on Human Factors in Computing Systems* (Seoul, Republic of Korea) (CHI '15). Association for Computing Machinery, New York, NY, USA, 67–76. doi:10.1145/2702123.2702497
- [53] James F. Steffe. 1996. *Rheological methods in food process engineering*. Freeman Press, N/A.
- [54] Xue Sun, Wenwen Deng, Xudong Wei, Dingyi Fang, Baochun Li, and Xiaojiang Chen. 2023. Akte-Liquid: Acoustic-Based Liquid Identification with Smartphones. *ACM Trans. Sen. Netw.* 19, 1, Article 18 (feb 2023), 24 pages. doi:10.1145/3551640
- [55] Rundong Tian, Christine Dierk, Christopher Myers, and Eric Paulos. 2016. MyPart: Personal, Portable, Accurate, Airborne Particle Counting. In *Proceedings of the 2016 CHI Conference on Human Factors in Computing Systems* (San Jose, California, USA) (CHI '16). Association for Computing Machinery, New York, NY, USA, 1338–1348. doi:10.1145/2858036.2858571
- [56] Yutaka Tokuda, Deepak Ranjan Sahoo, Matt Jones, Sriram Subramanian, and Anusha Withana. 2021. Flowcuts: Crafting Tangible and Interactive Electrical Components with Liquid Metal Circuits. In *Proceedings of the Fifteenth International Conference on Tangible, Embedded, and Embodied Interaction* (Salzburg, Austria) (TEI '21). Association for Computing Machinery, New York, NY, USA, Article 35, 11 pages. doi:10.1145/3430524.3440654
- [57] Cesar Torres, Molly Jane Nicholas, Sangyeon Lee, and Eric Paulos. 2019. A Conversation with Actuators: An Exploratory Design Environment for Hybrid Materials. In *Proceedings of the Thirteenth International Conference on Tangible, Embedded, and Embodied Interaction* (Tempe, Arizona, USA) (TEI '19). Association for Computing Machinery, New York, NY, USA, 657–667. doi:10.1145/3294109.3295643
- [58] Blase Ur, Melwyn Pak Yong Ho, Stephen Brawner, Jiyun Lee, Sarah Mennicken, Noah Picard, Diane Schulze, and Michael L. Littman. 2016. Trigger-Action Programming in the Wild: An Analysis of 200,000 IFTTT Recipes. In *Proceedings of the 2016 CHI Conference on Human Factors in Computing Systems* (San Jose, California, USA) (CHI '16). Association for Computing Machinery, New York, NY, USA, 3227–3231. doi:10.1145/2858036.2858556
- [59] Wen Wang, Lining Yao, Teng Zhang, Chin-Yi Cheng, Daniel Levine, and Hiroshi Ishii. 2017. Transformative Appetite: Shape-Changing Food Transforms from 2D to 3D by Water Interaction through Cooking. In *Proceedings of the 2017 CHI Conference on Human Factors in Computing Systems* (Denver, Colorado, USA) (CHI '17). Association for Computing Machinery, New York, NY, USA, 6123–6132. doi:10.1145/3025453.3026019
- [60] Yanan Wang, Shuai Liu, Yujia Lu, Jun Duan, Cheng Yao, and Fangtian Ying. 2016. Designing with Concrete For Enhancing Everyday Interactions. In *Proceedings of the 2016 CHI Conference Extended Abstracts on Human Factors in Computing Systems* (San Jose, California, USA) (CHI EA '16). Association for Computing Machinery, New York, NY, USA, 1497–1502. doi:10.1145/2851581.2892372
- [61] Yezhou Wang, Zhang Runting, Haonan Wu, and Guangtao Xue. 2021. Material Identification System with Sound Simulation Assisted Method in VR/AR Scenarios. In *Adjunct Proceedings of the 2021 ACM International Joint Conference on Pervasive and Ubiquitous Computing and Proceedings of the 2021 ACM International Symposium on Wearable Computers* (Virtual, USA) (UbiComp '21). Association for Computing Machinery, New York, NY, USA, 575–579. doi:10.1145/3460418.3480162
- [62] Michael L. Waskom. 2021. seaborn: statistical data visualization. *Journal of Open Source Software* 6, 60 (2021), 3021. doi:10.21105/joss.03021
- [63] Chenshu Wu, Feng Zhang, Beibei Wang, and K. J. Ray Liu. 2020. MSense: Towards Mobile Material Sensing with a Single Millimeter-Wave Radio. *Proc. ACM Interact. Mob. Wearable Ubiquitous Technol.* 4, 3, Article 106 (sep 2020), 20 pages. doi:10.1145/3411822
- [64] Humphrey Yang, Danli Luo, Kuanren Qian, and Lining Yao. 2021. Freeform Fabrication of Fluidic Edible Materials. In *Proceedings of the 2021 CHI Conference on Human Factors in Computing Systems* (Yokohama, Japan) (CHI '21). Association for Computing Machinery, New York, NY, USA, Article 620, 10 pages. doi:10.1145/3411764.3445097
- [65] Clement Zheng, Bo Han, Xin Liu, Laura Devendorf, Hans Tan, and Ching Chiuan Yen. 2023. Crafting Interactive Circuits on Glazed Ceramic Ware. In *Proceedings of the 2023 CHI Conference on Human Factors in Computing Systems* (<conf-loc>, <city>Hamburg</city>, <country>Germany</country>, </conf-loc>) (CHI '23). Association for Computing Machinery, New York, NY, USA, Article 474, 18 pages. doi:10.1145/3544548.3580836
- [66] Amit Zoran and Dror Cohen. 2018. Digital Konditorei: Programmable Taste Structures using a Modular Mold. In *Proceedings of the 2018 CHI Conference on Human Factors in Computing Systems* (Montreal QC, Canada) (CHI '18). Association for Computing Machinery, New York, NY, USA, 1–9. doi:10.1145/3173574.3173974